December 2017

Surface Alloying of Plain-carbon Steels During the Casting Manufacturing Process

Michael Beining
University of Wisconsin-Milwaukee

SURFACE ALLOYING OF PLAIN-CARBON STEELS DURING THE CASTING MANUFACTURING PROCESS

by

Michael Beining

A Thesis Submitted in

Partial Fulfillment of the

Requirements for the Degree of

Master of Science

in Engineering

at

The University of Wisconsin-Milwaukee

December 2017

ABSTRACT

SURFACE ALLOYING OF PLAIN-CARBON STEELS DURING THE CASTING MANUFACTURING PROCESS

by

Michael Beining

The University of Wisconsin-Milwaukee, 2017
Under the Supervision of Professor Pradeep Rohatgi

At times, the surface properties of an engineered component must be improved or enhanced when compared to the bulk of the component. Thus, various methods of surface alloying, one of the most important surface engineering processes, have been studied and developed for the decades. This study is concerned with the modification of the surface of WCB plain-carbon steel to improve corrosion and wear resistance of components used in the fresh water industry. The objective is to create a corrosion and wear resistant surface on an engineered component by enriching the surfaces with nickel or nickel and chromium, while the bulk of the component is composed of cheaper plain-carbon steel.

A unique, novel method for surface alloying has been created in this study, which involves the incorporation of metal powders of selected size into a slurry using a binder. This slurry was coated onto traditional sand cores prior to pouring the molten steel to produce the castings. The cores are placed in a sand mold, and the plain-carbon steel is cast, fills the mold, and comes in contact with the core, melting the alloying elements and rapidly solidifying them on the surface of the casting. Once solidified, the surface of the casting is expected to be enriched by with nickel or nickel and chromium on the surface.

Maynard Steel Casting Company in Milwaukee, WI assisted the project by casting the steel samples, and various UWM experiments were conducted using an induction coil capable of melting steel. Once the samples were prepared so that the cross-section of the WCB steel with the enriched layer could be analyzed, various analytical tests were conducted to demonstrate surface enrichment. Optical microscopy was used to view the quality and measure the depth of the surface layer, as well as to analyze the microstructure. The average thickness of the enriched layer for the successful trials was 339μm. An SEM was used to provide quantitative chemical analysis of the samples, which showed a chemical composition on average of 19% chromium and 7% nickel, with an iron balance. X-ray diffraction was used to investigate the phases present in the surface, which showed the presence of austenite and ferrite, similar to the diffraction pattern of CF3 stainless steel. Microhardness tests show that the surface has an average hardness of 484 HV500, while plain-carbon steel has a hardness of 155 HV500, indicating a greater wear resistance for the enriched surface. The rate of corrosion of the surfaces enriched with nickel and chromium showed a range of 0.066 – 0.087 mm/yr, while typical plain-carbon steel showed a rate of 0.609 mm/yr, indicating the enriched surface is 10.8 - 14.0 times more corrosion resistant than the base steel. This indicates that surface enrichment has occurred during this casting method, and the wear resistance increased as well as the corrosion resistance.

TABLE OF CONTENTS

LIST OF FIGURES

ACKNOWLEDGEMENTS

During the time I spent on this research, I have had the opportunity to work with academic achievers from multiple continents around the globe. From the United States, to India, to Iran, to China, to Turkey, I am grateful for the professional and personal relationships I have made with my colleagues and classmates. I would first like to acknowledge Professor Pradeep Rohatgi, my research advisor, who has guided and motivated me on this project. He has also taught me about the science of metal casting and solidification, and has helped me to gain an interest in the metal casting industry. I would also like to thank the Water and Equipment Policy (WEP) and I/UCRC for funding this project for two years. Thank you to Dr. Afsaneh Dorri for giving advice and ideas, which has helped me to further my research, and for your assistance and support in the Advanced Analysis Facility. Thank you to Mr. Emad Omrani and Mr. Behnam Gohari for your professional input, advice, support and friendship. I would also like to thank Mr. Swaroop Bahera and Mr. Sourav Das, my current teammates who have helped me with various projects and throughout the semester. Thank you to Dr. Hathibeligal Roshan for your advice and guidance, and to Maynard Steel Casting Company for helping advance this project. Thank you Mr. Kyle Brown for helping me any time I would need it. I would like to thank Dr. Nathan Salowitz, Dr. Ben Church, and Dr. Ben Schultz for serving on my thesis defense committee. I appreciate the support and guidance from you all. And finally, thank you to my parents, Mike and Debbie Beining, my sister Katie Beining, my sister Kari Pollard, my brother-in-law Kevin Pollard, and my nephews Joey and Jack Pollard. I appreciate all of the support that you have all given to me.

1. Introduction

The goal of this study is to investigate a new process for modifying the surface of a material, and to see how this surface affects selected properties of the component. The base material that was surface modified was WCB grade plain carbon steel, and the alloying elements that were chosen to enrich the surface of this base alloy steel were nickel and chromium. By changing the chemical composition of the surface, the corrosion resistance and wear resistant properties became enhanced, and therefore replace expensive components made out of stainless steel with this new technology. The scope of this novel research project included the following items

1. Research a new way to achieve surface alloying via the sand casting method
2. Select the right alloying elements that would help enhance corrosion and wear resistance
3. Create the optimum binder and metal powder sizes and mold coating procedures to achieve surface alloying in laboratory and industrial scale experiments
4. Characterize the surface enriched samples using various analytical techniques for changes in surface composition and structure
5. Measure the corrosion and hardness properties of the samples

The initial challenge was to discover a way to transfer the alloying elements to the surface of the desired component, in a reproducible way that ensured a continuous coating. Once

that method was achieved, the next task was to characterize the surface chemistry and other properties of the samples. Throughout the course of this thesis, the reader will be able to follow the methodology of how the surface enrichment took place, how the various complications of the initial experimentation were overcome, and what characterization methods were used.

2. Literature Review and Background

2.1 Steel Alloys

The processes used to successfully achieve nitriding and carburizing in ferrous alloys have been well studied and achieved both in the laboratory and in the industry. Instead of producing a modified layer on the surface steel using techniques suitable for nitriding or carburizing, the goal of this work is to achieve a metallic layer metallurgically bonded to the steel during the casting process itself. A unique method for coating sand cores with powdered elemental chromium and nickel prior to casting WCB steel has been developed. The target of this project is to achieve a chemistry of CF3 stainless steel on the surface of the WCB steel during casting, and to investigate and analyze the chemical and physical properties the samples.

The use of quality steels of all grades is in high demand for applications in the freshwater industry. Plain carbon, WCB grade steel castings are utilized for components like valves, fittings, flanges, and pump casings, and are suitable for both low and high temperature applications[1]. According to ASTM-A216, WCB is acceptable for use in the temperature range of -20°F to 800°F for freshwater applications. WCB has a good combination of strength and ductility, with a tensile strength of 70,000 psi, a yield strength of 36,000 psi, and a 26% elongation[2].

In addition to its attractive physical properties, at $0.79/pound on the market today, it is inexpensive compared to its stainless steel counterparts. It has excellent castability and forgability, and can easily be welded and machined[3]. In addition, this alloy can be heat treated by annealing or normalizing to further improve the mechanical properties. This allows for WCB to be an advantageous material selected for many industries that require strong, low-cost applications, but this study will be focused primarily on components used in the water industry. The ASTM chemistry specifications for WCB are listed below in Table 1[4].

Alloy	Carbon %	Manganese %	Copper %	Nickel %	Chromium %	Fe %
WCB	0.3% Max	1.0% Max	0.3% Max	0.5% Max	0.5% Max	Bal
CF3	0.03% Max	1.5% Max	1.0% Max	8.0-12.0%	17-21%	Bal

Table 1: WCB and CF3 Alloy Compositions

The CF3 alloy is the most versatile and widely used alloy in the stainless steel family[5]. Referred to the standard '18/8 stainless', this material is utilized in a wide variety of applications, including food processing equipment, particularly beer brewing, milk processing, kitchen appliances, architectural applications, nuclear applications, high-temperature applications, automotive and aerospace applications, heat exchangers, chemical containers, and components in pumps as well[6]. The incorporation of chromium and nickel (particularily around

18% chromium and 8% nickel) in this alloy is what makes it stainless, meaning the chromium produces a protective layer of chromium oxide when exposed to moisture, hindering the rate of corrosion[7]. This allows for the material to be used in harsh oxidizing environments, such as in seawater, or exposure to acids. Fresh water also promotes oxidation, which is why this alloy is used for fresh-water valves and pump casings.

In addition to the good corrosion resistance, CF3 (and other grades of stainless steel) possess mechanical and physical properties very similar to that of WCB and other low-carbon steel alloys. According to the ASTM-A351 standard for CF3, the tensile strength is 70,000 psi, the yield strength is 30,000 psi, and the elongation is 35%, giving a greater ductility than WBC[8]. Although the physical properties of CF3 are as good as WCB, it is three times as costly. The price for this alloy is $2.80/pound, which is due to the expensive qualities of nickel and chromium. The chemistry of the CF3 alloy is listed below in Table 1[9].

The driving factor behind this research project is to utilize a low-cost bulk material, such as WCB, which inherently possesses good mechanical properties, and modify only the surface of it to enhance the corrosion resistant and hardness properties. This will be beneficial in the freshwater industry because components like valves and flanges, which are already made of cast WBC, will have enhanced corrosion and wear resistant surfaces which are in contact with the water, while the rest of the component is made from cheaper material. The cost of the surface alloyed component should be cheaper than a component cast from 100% CF3. The current methods of laser alloying, laser cladding, and plasma nitriding are relatively expensive methods of surface modification, which is why a cheaper casting method has been considered. The ideal component should have a uniform, adherent layer, with chemistry close to that of CF3 stainless steel, which will increase the physical and chemical properties without compromising cost, which is the goal of this project.

2.2 Carburizing

One of the oldest surface hardening methods, dating back 3000 years ago[10], is carburizing, which is now a well-understood and established process. Carburizing involves diffusion of the element carbon into the surface of the substrate, which results in an increase in hardness of the surface layer. When steel is placed in a carbonaceous environment for a period of time at an elevated temperature, the carbon diffuses into the steel matrix due to a concentration gradient that exists[11]. Although the carburizing media is in solid state, there is not a solid-solid interaction between the steel and the carbon. Instead, oxygen in the air reacts with the carbon in the carburizing media, and the following reactions occur:

$$C + O_2 \rightarrow CO_2$$

$$2C + O_2 \rightarrow 2CO$$

When the temperature rises, the following reaction occurs and the equilibrium shifts toward the right. Thus, the gas becomes richer in CO, and at a temperature at or greater than 800°C, the following reaction occurs:

$$CO_2 + C \leftrightarrow 2CO$$

Which is commonly known as the 'Boudouard reaction'[12]. At the steel/gas interface, the decomposition of carbon monoxide gas occurs via the following reactions:

$$2C + O_2 \rightarrow CO_2 + C_{atomic}$$

$$Fe + C_{atomic} \rightarrow Fe(C)$$

where near the surface of the steel, Fe(C) is the carbon that is dissolved and diffused into the austenite phase. Because of the size difference between the iron and carbon, and due to the concentration gradient and high temperature, carbon readily dissolves into the steel surface[12]. An increase in temperature, time, or the amount of carbon present will also increase the rate of the reaction and amount of carbon diffused. Carburization is a 3000-year-old technique that is still used today to increase the hardness of the surface of steel and increase its wear resistance. One of the objectives of this study is to investigate and determine if the surface produced through surface alloying with chromium and nickel will achieve a harder surface, although the reason for the increase in surface hardness may be different than through carburization.

2.3 Laser Surface Alloying

Laser surface alloying is a method used to modify the surface properties of a material without affecting its bulk properties[13], and is used especially for titanium alloys used in the biomedical sector[14]. Titanium is a favorable material to be used in the body due to its good biocompatibility, corrosion resistance, and a high specific strength similar to that of human bone[15]. The major downfall of titanium is its lack of hardness and poor wear resistance. However, laser remelting of titanium in a nitrogen-containing environment, also known as laser gas nitriding (LGN), and gained popularity for increasing the wear resistant and hardness properties of titanium[16]. Similar wear resistance and increased hardness findings have been discovered in aluminum alloys which have undergone laser surface alloying[17].

Some of the advantages of using LGN over other diffusion-based surface treatments include being able to deliver large power/energy densities (103-105 W/cm^2), a high heating to cooling rate (103-105 K/s), and high solidification velocities (1-30 m/s). The surface microhardness increased nearly four times when subjected to this method of laser alloying

compared to the non-laser treated substrate[14]. Typically, a laser, along with a supply of powder entrained in a carrier gas, passes over the surface of the metal substrate[18]. The heat generated by the laser immediately melts both the powder and the metal substrate, and once it passes over that region, the two solidify rapidly[19]. There are high rates of deposition with this method, as well as a low heat affected zone, and a refined microstructure as a result. The major downfall is the high cost of using this method, as well as requiring non-complex geometries of components. There is also a limitation in the thickness of the surface alloyed layer using this technique[20]. Figure 1 below shows a typical setup schematic for laser surface alloying.

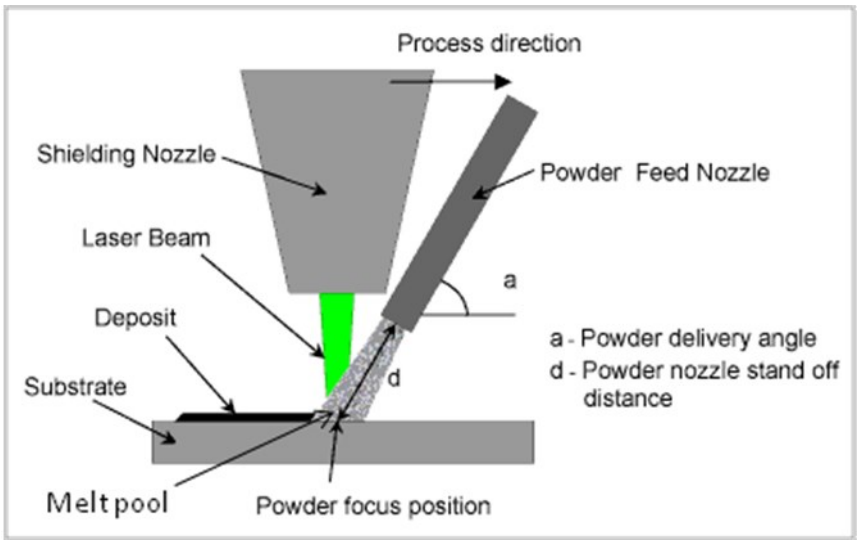

Figure 1[21]**:** The schematic diagram of a laser alloying operation.

Other alloying elements that are typically used in laser surface alloying processes are usually metals, such as cobalt, chromium, magnesium, nickel, and tungsten. Ceramics, such as carbides, nitrides, and borides, as well as nickel-based superalloys, are also used in laser surface alloying[22].

2.4 Friction Stir Welding

Another emerging surface engineering method is friction stir welding, which has been successful at surface alloying aluminum, copper, iron, and nickel based alloys. Capable of reducing or eliminating casting defects, this process is capable of improving strength, wear, and fatigue properties[23]. Microstructural refinement is also a beneficial byproduct of friction stir processing[24]. This method involves plunging a rapidly spinning, hard consumable drill bit tool, which consists of the alloying element which is desired to be deposited onto the surface, into the surface of the metal component, and then traversing the bit across the surface. Figure 2 below[25] shows a schematic for a friction stir weld process. The rotating pin moves at a high velocity, and is dragged along the length of the junction, creating the weld.

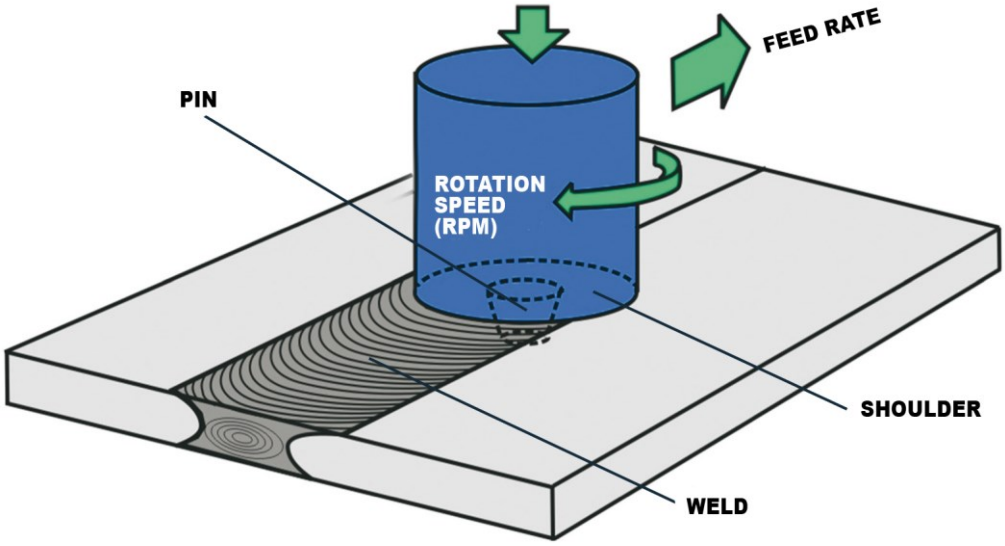

Figure 2: Diagram of a friction stir welding set-up. *http://www.uqac.ca/ceeuqac*

When the pin dragged along the surface, extreme heating and plastic deformation occurs, causing the metal to flow around the bit and solidify in the bit's wake. Aluminum metal matrix composites (MMCs) consist of an aluminum matrix reinforced with ceramic materials[26]. They exhibit properties better than either parent material, including strength, elastic modulus, wear resistance, creep resistance, and fatigue resistance[27]. They are promising materials for

aerospace and automotive industries. By modifying the surface of these aluminum MMCs, they can become surface metal matrix composites (SMMCs), which exhibit a hard, wear resistant surface, and a ductile substrate[28].

Solid-state processing methods like friction stir welding are favorable because they do not require the formation of liquid state during manufacture, and produces very fine, equiaxed, homogeneous grain structures[28]. In the liquid state, the formation of some detrimental phases on the surface could occur during solidification of these SMMCs. Friction stir welding is a good choice in fabricating these composite materials, as it is entirely solid-state. The bonding of SiC and TiC particles on the surface of aluminum alloys has been successful, with a good particle bond with the metal matrix[29].

2.5 Plasma Source Ion Implantation

Another method of surface modification, plasma source ion implantation (PSII) is similar to traditional ion implantation, but this new cost-efficient modification forms an ion sheath around the substrate, and then bombards it with ions[30]. It uses a pulsed power supply with a maximum voltage of 25 kV and a current of 10 A with frequencies varying from 10 to 5 kHz[31]. PSII can be combined with thin film deposition systems as well, and may be used with nonreactive or reactive gasses, forming compound films.

In comparison with plasma nitriding, PSII treated stainless steels show better properties, although the cost for using PSII is higher[32]. In the case of austenitic stainless steels, PSII provides a wear resistance three times higher than the untreated counterpart, with no loss in the good corrosion resistant properties. Ion implantation is regularly applied to harden surgical prostheses before implantation into the body, making it a favorable technique in surface modification of biomedical devices[33].

2.6 Sand Casting Method

Surface modification by means of any casting method, including sand, permanent die, continuous, or investment, have not been taken into consideration. The process that this project focuses on is the enrichment of a steel surface by means of sand casting. It is not a diffusion-driven process like carburizing, nitriding, siliconizing, and chromizing, nor is it a melted-on, welded, or ion-bombarded process. Unlike the pricey, geometrically constrained methods like friction stir welding and ion-nitriding and implantation, this method uses the simplicity and inexpensiveness of sand casting to achieve an enriched surface layer. The following section explains the experimental methodology to achieve the desired results.

3. Experimental Section

The major experimental efforts for this study consisted of designing and perfecting a unique method to enrich the surface of WCB steel during the casting process, specifically sand castings both in an industry setting and experimentally in the Foundry Laboratory as well. Under the guidance of Dr. Hathibeligal Roshan of Maynard Steel Casting Company in Milwaukee, WI, two industrial heats were made during the course of this study. The unique method of enriching the surface of the castings involved creating a slurry with an appropriate binder that was mixed with powdered alloying elements of fixed mesh sizes. The objective was to create a suitable slurry that would effectively stick to the sand mold upon drying after application, and would allow for the molten steel to melt the powdered alloying elements during casting, leaving a good surface finish with a coherent surface alloyed layer. The details of both heats conducted at Maynard Steel, as well as all of the UWM Laboratory trials, are detailed in the following subsections.

3.1 First Maynard Heat and Set of UWM Experiments

Often times, sand casting operations utilize the use of cores inside their molds to achieve products of complex geometries. Typically made from sand, a core is a rigid structure that forms the interior portion of the sand mold. The interior part of the sand mold gives an area for the metal to flow, while the core creates the negative of the desired product, as the metal cannot flow into any area occupied by the core. Since components used in the freshwater industry, such as pumps and valves, almost always require the use of cores in their sand molds, and because the surface that comes in contact with water and is therefore desired to it enrich touches the sand core while molten during casting, was decided to apply the slurry directly to the sand core prior to casting.

The slurry in consideration, which would be applied directly to the sand core, had two critical requirements that needed to be considered. First, it needed be made with a binder that would appropriately adhere to the surface of a sand mold, while also allowing for the alloying elements to release during the casting process when it came in contact with the molten steel. Secondly, the slurry needed to contain alloying elements that were in powder form, would effectively melt below the melting temperature of WCB steel, and would give rise to advantageous properties on the surface after casting.

Maynard Steel Company provided Refcohol 1010 refractory wash to be used as a binder for the slurry prior to the first heat being poured. This zircon-based wash, which is applied to the interior of the sand mold, along with the any cores inside of it, is alcohol based, protects the sand from sand burn on, prevents reactions from happening between the molten metal and the sand, and gives a good quality finish to the final product. It is always necessary to apply a refractory wash to the interior of sand molds in an industry setting. Since refractory wash is commonly used in sand foundries, it made for an acceptable first choice of a binder material in the slurry.

The sand cores were provided by Maynard Steel and were made from no-bake sand. They were ¾" tall, the bottom circular diameter measured 2" and the top diameter measured 1". Figure 3 below shows 12 sand cores, along with the mold that they were made in.

Figure 3: Core box and 8 uncoated sand cores provided by Maynard Steel

The alloying elements that were chosen to coat the cores were copper and nickel for this initial heat at Maynard Steel. Copper inherently possesses good corrosion-resistant properties, and nickel is added to stainless steel for its good corrosion-resistant properties too. The two elements were ordered from Sigma Aldrich with a mesh size of <50 μm, and a purity of 99.5%. A design of experiments was used with three variables, and a low and a high value for them, giving a combination of 3^2, or 9 different possibilities. Table 2 below gives the details of the design of experiments for the first round of samples cast at Maynard Steel.

Factor	Low Level (-1)	High Level (+1)
Composition	3g Ni	6g Ni
Mass of Baked-on Wash	15g	30g
Copper Addition	0g Cu	3 Cu

Table 2: Design of experiments for the first heat poured at Maynard

Initially, 20 mL of industry wash was used as the binder, and then various amounts of powders were added, depending on the level for each factor. Once the powders were added to the wash, they were mixed by hand until they solution was homogeneous. A paintbrush was then used to carefully add the correct amount of slurry onto the sand core. Once the slurry was added to the core, it was ignited with a blowtorch to dry and solidify it. The mass was taken after the slurry was dried to make sure that the core contained the correct amount based on the level. If there was not enough slurry, more was added with the paintbrush and it was again ignited. If too much was added, some of the hardened slurry would be removed carefully by rubbing the top of it with 600 grit sandpaper. The tops of all of the samples were carefully rubbed with 600 grit size sandpaper, and then marked accordingly. Figure 4 below shows the top of a sand core on fire after being ignited, and figure 5 shows the dried slurry containing the alloying elements and industry wash on 8 cores.

Figure 4: The top of a sand core that has been ignited with a blowtorch.

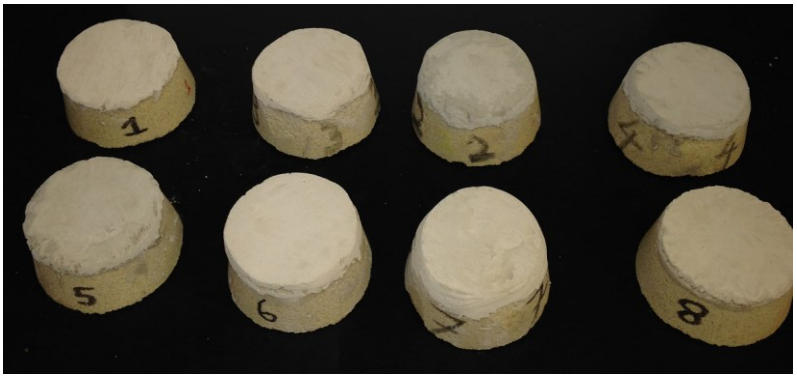

Figure 5: Eight cores with alloying element-containing slurry hardened on top of them. The tops of the cores had been smoothed with sandpaper.

Once all of the cores were prepared, they were delivered to Maynard Steel for casting. The cores were placed inside the middle of a rectangular test block pattern inside a large mold. Figure 6 illustrates the cope and drag in which the cores were placed, and Figure 7 shows the cores placed inside the drag side of the mold.

Figure 6: The cope and drag of the sand molds in which the cores were placed.

Figure 7: The drag side of the sand mold with the sand cores placed inside the test cavities. The mold was then closed, and steel was cast into it.

Once the cores were placed into the test cavities and the mold was shut, it was time to cast the steel. The WCB was brought to a temperature near 1600°C and poured into the mold.

After that, the samples were shot-blasted and normalized, and were then sent to UWM for analysis.

Each sand core cavity was capable to filling up ten pounds of steel, and Figure 8 shows the test block with the supposed enriched surface. The center was cut out into a small cube, as the center face is the one that was enriched. The UWM machine shop cut the samples with a band saw, and a metallographic abrasive saw was used to cut them into smaller cube samples. Figure 9 shows where the sample was cut out so that the cross-section could be observed.

Figure 8: The ten-pound test block. The enriched surface is the one that came in contact to the slurry, which is the flat, recessed surface that is visible.

Figure 9: The center cube was cut out from the test block. This sample was mounted in such a way that the cross-section from the surface into the substrate could be studied.

The samples were then taken to a mounting machine and were mounted in black phenolic powder. They were then ground with silicon carbide paper with grit sizes 320, 400, 600, 800, and 1200. After that, they were polished with 0.5 micron sized alumina, and were then etched for 5 seconds with 3% Nital solution. The samples were then subjected to various characterization tests, including optical microscopy, a scanning electron microscope (SEM), energy dispersive spectroscopy (EDS), microhardness tests, X-Ray Diffraction, and finally potentiodynamic polarization test.

Meanwhile, as the samples were being poured at Maynard Steel, experiments were being conducted in the foundry laboratory at UWM. The same principle of coating cores with a slurry was being utilized, but in this case, a small vacuum induction furnace was used to melt the steel. A quartz tube closed system apparatus was designed so that no physical pouring was done. Instead, pieces of WCB steel were placed inside a small graphite crucible with a hole drilled out of the bottom. A coated sand core was then placed underneath the hole so that upon melting, the steel would drip directly on top of the sand core, allowing for the alloying elements to be released onto the surface of the molten steel. A hollow graphite spacer was placed between the

crucible and the coated core. Below the core, Kaewol was placed for safety incase some of the steel ran off and fell below the core, although this run-off never happened in any of the experiments. All of these casting components were placed inside a quartz tube, which was then attached to a vacuum pump. Figure 10 is a picture of the quartz tube with all of the components inside.

Figure 10: The quartz tube with all of the components used for casting in a small induction furnace.

Once all of the components of the melting set-up were placed inside the quartz tube, it was then connected to a vacuum pump and brought to a low vacuum condition. This ensured that oxidation would be at a minimum when the metal became molten and dripped onto the core. The induction furnace was then turned on, and the voltage was slowly ramped up at a rate of 15 amperes/minute, until it reached 210 amperes, and was held there for 2 minutes. After that, the power to the furnace was shut off, and the sample was allowed to cool. Figure 11 shows the glowing red-hot quartz tube while the steel was being melted, and the vacuum pump on top of it.

Figure 11: The red-hot quartz tube on the vacuum pump as the steel is being melted.

The setup was such that the induction coils were positioned so that they heated up the portion of the tube that contained the crucible with the steel pieces in them. After the metal fell onto the core and solidified, it was taken out of the tube and mounted and prepared the same way that the Maynard Steel samples were, so that they could undergo the same characteristic analysis.

3.2 Second Heat at Maynard Steel with New Slurry Design

After the first trial of Maynard Steel samples and UWM samples were shown not to be enriched in the surface, a new binder material for the slurry was explored. The previous industrial wash binder did not allow for release of the alloying elements into the surface, so two other binders, methylcellulose and sodium polyacrylate, were considered. Both of these have been used for casting applications as binders, so both of the chemicals were purchased from Sigma Aldrich.

It was decided that water was to be added to either of these chemicals to create the slurry in which powdered metallic alloying elements would be incorporated into. The methylcelluse was considered first, and when water was added to it, the methylcellulose did not absorb any of the water, and was simply suspended in it. The methylcellulose seemed to have no reaction with the water when stirred, shaken, or was allowed to set for a period of time. Therefore, the second potential binder chemical, sodium polyacrylate, was tried. This chemical is the active absorbent material in diapers, and is very efficient at absorbing and retaining liquids. Initially, 4 grams of sodium polyacrylate were attempted to be dissolved into 100 mL of distilled water. This was discovered to be a more than sufficient amount of powder, as see in Figure 12.

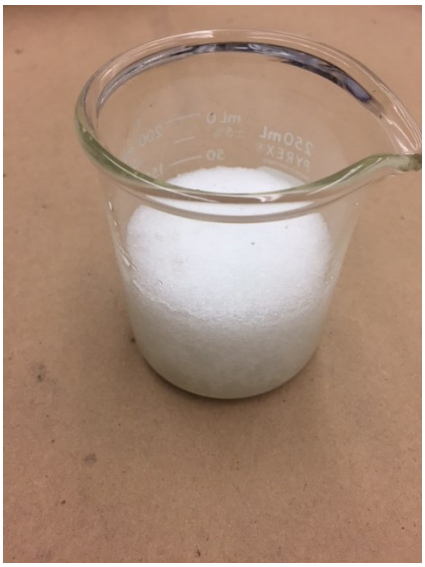

Figure 12: The results of adding 4g sodium polyacrylate to 100 mL of water. The water became supersaturated almost instantly, and a lesser amount of binder was required.

After various experiments were conducted to determine the appropriate binder-to-water ration, it was determined that 0.3g of sodium polyacrylate being added to 100mL of water was sufficient. The solution was then placed in a Resodyn acoustic mixer and mixed at 80% intensity for 2 minutes to allow for a homogenous, viscous solution to form. Figure 13 shows the water and binder material solution after it has been acoustically mixed for two minutes.

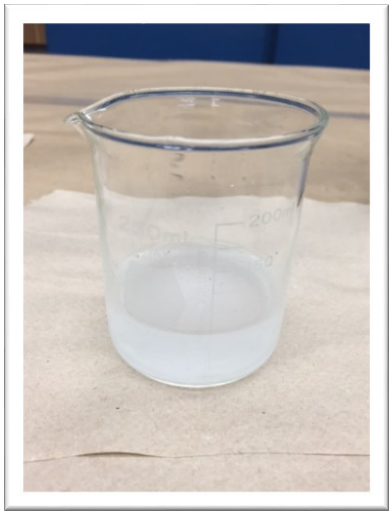

Figure 13: The sodium polyacrylate and water solution after it has been acoustically mixed for 2 minutes. The solution is not ready for addition of alloying element powders.

Once the binder material was mixed acoustically, powdered nickel was ready to be added to the solution to create the final slurry. It was decided that copper was not going to be added for the second heat at Maynard Steel, because copper generally is not present in large quantities of corrosion-resistant grades of steel. For the second heat at Maynard steel, there were 8 cores prepared with nickel powders. Four cores had the same amount of nickel present, 8 grams, while the other four had 10 grams. The cores were prepared and dried in a low-temperature furnace at 70ºC for two hours. The resultant slurry coating appeared smooth, uniform, and covered the entire surface. Figure 14 shows the slurry-coated core before it was placed in the furnace for drying.

Figure 14: The slurry-coated core still wet before drying in a low-temperature furnace.

Once the cores were dried properly and examined to make sure that the slurry on the surface was smooth and continuous, they were sent to Maynard Steel for a second heat of casting. Meanwhile, in the lab, experiments with powdered copper were being conducted to see if the slurry would release the alloying element into the substrate upon casting. The same induction melting setup was used, and this time, a core coated with copper powder in the sodium polyacrylate binder was places beneath the spacer and crucible containing the steel. The sample was removed after the steel was poured onto the surface, and was cross-sectioned and examined to determine if the slurry released the powder. Figure 15 shows the cross-section of the sample containing 45 grams of WCB steel interacting with 18 grams of copper powder slurry, and figure 16 shows a stereomicroscopic image of the interface between the substrate and the copper at 8x magnification.

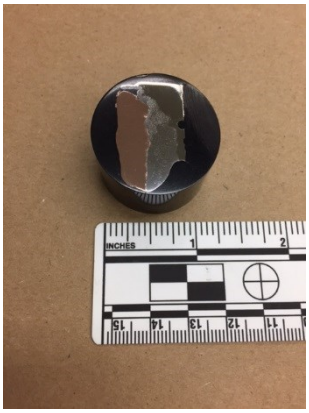

Figure 15: The mounted sample of copper and steel made by induction melting in the UWM foundry lab.

Figure 16: The stereoscopic image of the steel sample enriched with copper, 8x magnification.

3.3 Third Heat with Stainless Steel Composition

The results from the second heat at Maynard Steel gave a promising result that an enriched layer of nickel powder was achieved. This gave the indication that the design of slurry was successful, and for the third heat at Maynard Steel, it was determined to use chromium as well as nickel, to give the surface a composition similar to that of CF3 grade stainless steel. Since consistent reproducibility is a major factor when transferring this technology to an industrial operation, all eight cores were coated with the same amount of chromium and nickel powder. 20 grams of chromium and 8 grams of nickel were added to approximately 7-8 mL of

binder solution and mixed by hand, so that the powders were just saturated enough with the solution to stick to the sand cores. The slurry was carefully applied using a tongue depressor and a metallic spatula, so that the slurry was evenly distributed with a good surface finish. The cores were then placed in the furnace at 70ºC for two hours to allow for proper drying and adhesion to the sand. Figure 17 shows the dried sand core containing nickel and chromium powders after removal from the furnace. The surface has an evenly distributed coating of slurry that is adhered to the sand core.

Figure 17: The dried on nickel and chromium slurry prior to delivery to Maynard Steel.

Once all eight cores were coated with the slurry, they were given to Maynard Steel for casting. Meanwhile, more laboratory experiments using the latest nickel and chromium slurry design were conducted in the induction furnace. Four laboratory specimens were produced in the time between the delivery of cores to Maynard until the castings were received back at UWM. The following chapter will discuss the methods used to test and characterize the samples to indicate whether or not enrichment of the surface during casting occurred.

4. Results and Discussion

4.1 Sample Organization

In this section, the discussion regarding the organization of the samples will be clarified. In the first heat at Maynard Steel, two samples will be analyzed to determine if enrichment occurred. In the second heat, four samples were selected for analysis, and in the third heat, four samples were also selected for analysis. Maynard Samples #1 and #2 correspond with the first heat, Maynard Samples #3, #4, #5, and #6 correspond with the second heat, and Maynard Samples #7, #8, #9, and #10 correspond with the third heat. Additionally, UWM Samples #1 and #2 were made using the first industrial wash-based slurry, and UWM Samples #3, #4, #5, and #6 were made using the sodium polyacrylate-based binder, and were selected for analysis.

4.2 Optical Microscopy Results

The use of an optical microscope was beneficial in examining microstructures, as well as measuring the thickness of the enriched surface layer. For Maynard Samples #1 and #2, which underwent the normalizing heat treatment, it can be expected that pearlite and ferrite will be present in the WCB steel matrix, based on conclusions drawn from the time-transition-temperature curve for steel. Figure 18 shows the microstructure of Maynard Sample #1.

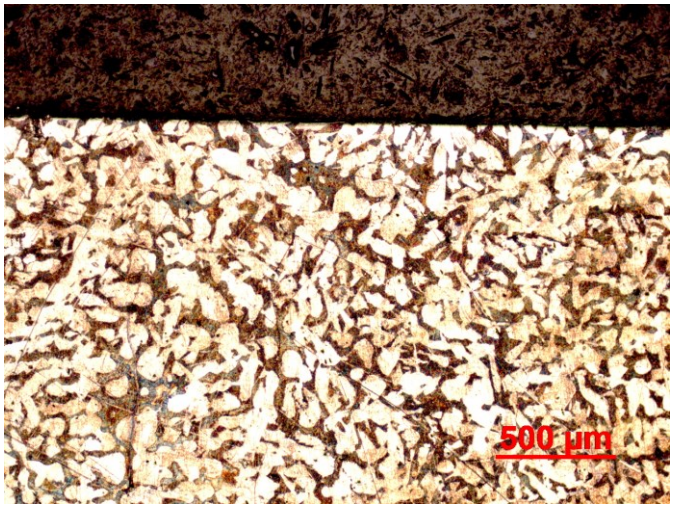

Figure 18: The surface of Maynard Sample #1. Dark phases of pearlite should be expected, along with light phases of ferrite, as this sample was normalized.

The results here indicate that there is no visible enrichment layer present of Maynard Sample #1. In addition, the first set of UWM induction experiments shows no surface layer as well. Figure 19 shows the microstructure of the UWM Sample #1. It was apparent then that the design of the first slurry using the industrial wash was a failure, and that no enrichment had occurred along the surface. EDS chemical analysis was able to confirm this as well.

Figure 19: The surface of UWM Sample #1 showing pearlite and ferrite in the microstructure, although no surface layer is evident.

Once it was realized that the industrial wash-based slurry was a failure, and once the new slurry using sodium polyacrylate was created and implemented, the second trial at Maynard Steel using only nickel powder was cast. The samples were received, and once again examined under an optical microscope. Figure 20 shows the microstructure, as well as the surface measurements, of Maynard Sample #3. The microstructures of Maynard Samples #4, #5, and #6 are shown in Appendix 2.

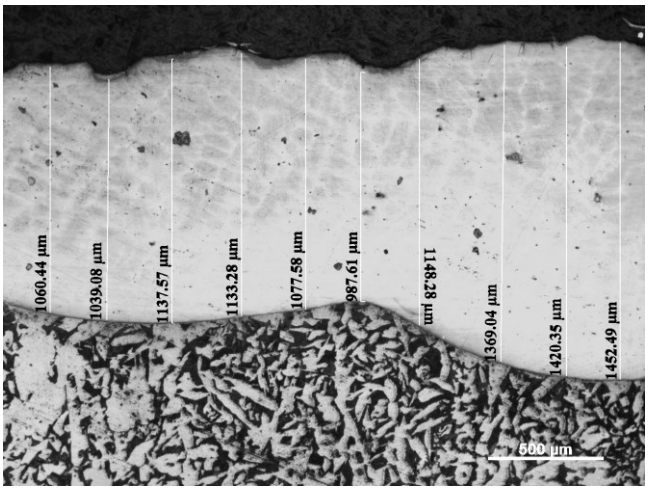

Figure 20: The microstructures of the surface and the substrate of Maynard Sample #3.

Once again it is apparent that the microstructure of the substrate is ferrite and pearlite based on the premise of normalizing heat treatment[34]. The surface is more difficult to view, but it may be a martensitic structure, as the surface alloying powders could have acted as a chill, solidifying the surface rapidly and causing a martensitic microstructure to appear. It is also possible that there is an austenite phase present, as nickel acts as an austenite stabilizer[35].

The third and final trial at Maynard consisted of chromium and nickel powders used in the slurry. Figure 21 shows the microstructure of Maynard Sample #7, enriched with chromium and nickel. Once again, the substrate shows ferrite and pearlite structures, and the highly reflective and shiny surface layer, which is difficult to etch. It could be expected that the

microstructure of the layer could consist of austenite and ferrite, as nickel is an austenitic stabilizer, and chromium is a known ferrite stabilizer. The microstructures and surface measurements of Maynard Samples #8, #9, and #10 are presented in Appendix 2.

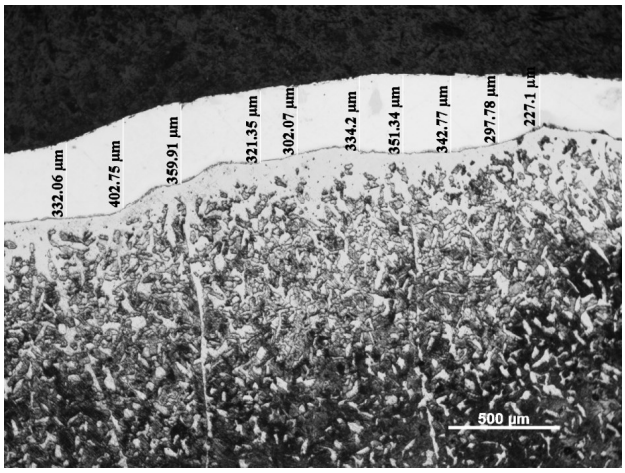

Figure 21: Microstructure of surface and substrate of Maynard Sample #7.

The final samples made at UWM had the same chemical composition on the surface of the sand core as the ones used in the last trial at Maynard. Figure 22 shows the microstructure of UWM Sample #3, which shows similar structures in the substrate and on the surface. UWM Samples #4, #5, and #6 are presented in Appendix 2.

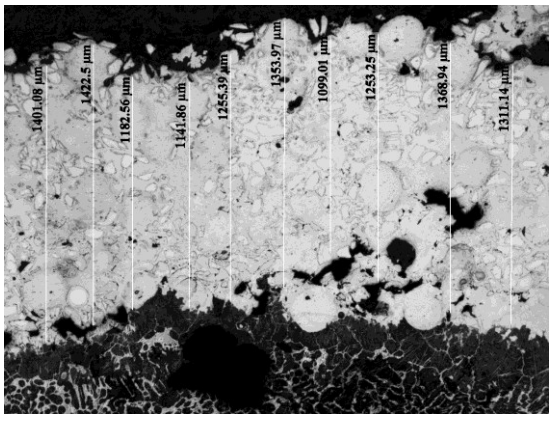

Figure 22: The microstructure the surface and substrate of UWM Sample #3.

The surface measurements are also able to be observed under the optical microscope. Table 3 below shows the average surface thicknesses for the Maynard Samples. The UWM Samples were not practical to take surface measurements of, because the quality of the surface in terms of smoothness was far less than the quality of the cast Maynard samples.

Maynard Sample	Average Thickness (µm)
3	1342
4	1298
5	1387
6	1423
7	342
8	297
9	319
10	325

Table 3: The average thickness of the alloyed layer in Maynard Sample #3 - #10.

It is apparent here that the average thickness of the first four only nickel Maynard samples produced a thicker layer, compared to the next four nickel and chromium samples. 30 measurements were taken for each sample to ensure a large amount of readings and a more accurate measurement of the surface.

4.3 SEM and EDS Results

Scanning electron microscopy (SEM) is one of the most popular techniques to examine and characterize metallic specimens, including those that are subjected to surface engineering. Instead of using light waves to view a sample, it bombards the surface of the sample with electrons, which provide a high-resolution image of the surface[35]. Magnifications are capable of

achieving up to 1,000,000x, while optical microscopes are limited to around 1,000x magnification. For the SEM used in this study, the incident electrons had energies of 15keV.

The SEM can image the surface by bombarding and scanning it with a beam of high-energy electrons. When the beam raster scans the sample, secondary or back-scattered electrons are excited and produced, which are collected by detectors[36]. The electrons are then converted to a voltage, amplified, and then displayed as an image on a computer screen. The SEM is able to provide surface topographical information as well as quantitative chemical analysis of crystalline samples. When the incident high-energy electrons are passed over the sample, characteristic x-rays are generated by the atoms within an element[37]. Each element has its own characteristic x-rays, which gives rise to the capability of using an SEM to perform quantitative chemical analysis. When the high-energy electrons hit the surface, they knock out inner shell electrons, in which case outer shell electrons move into the empty electron orbit of the sample[38]. At this stage, X-rays are emitted to balance out the conservation of energy. The measurements of these x-ray energies, or the wavelengths, can provide chemical information about the specimen. These x-rays are measured and detected by an energy dispersive X-ray spectrometer, or EDS. An EDS was used in this study to examine the chemical composition of the samples. Figure 23 shows the SEM image of the surface of Maynard Sample #3, as well as the EDS chemical results.

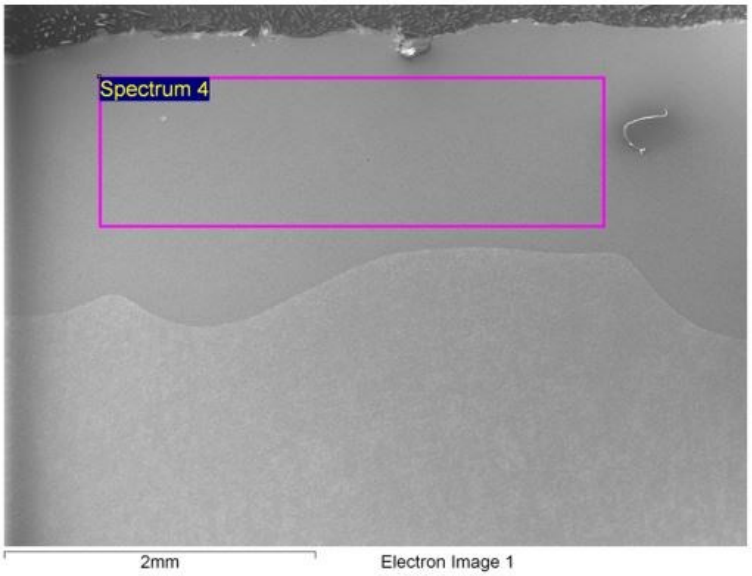

Sample #3

Element	Weight %	Atomic %
Fe	83.23	84.68
Ni	16.32	14.49
Si	0.45	0.83
Total:	100	100

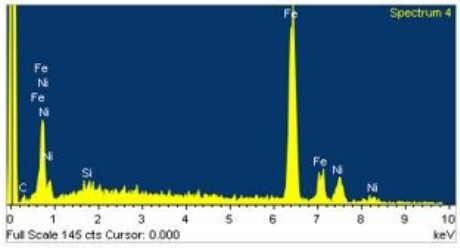

Figure 23: Chemistry, EDS spectrum, and area analysis of surface of Sample #3, cast at Maynard Steel. JOEL SEM, 27x, WD 12mm, accelerating voltage of 15 keV.

It can be seen here that the nickel enrichment at the surface is 16.21%, with a balance of iron. Figure 24 shows the SEM image and EDS results of the substrate of Maynard Sample #3. Here, the steel substrate is almost entirely iron, with no presence of nickel. This indicates that no diffusion of nickel into the substrate layer occurred during casting. The results of the SEM and EDS analysis for Maynard Samples #4, #5, #6, and #7 are presented in Appendix 1.

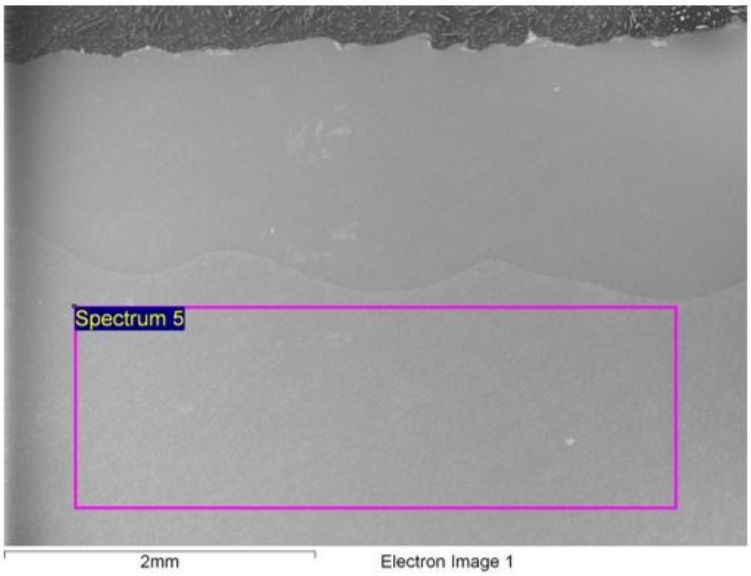

Sample #3

Element	Weight %	Atomic %
Fe	99.82	99.74
Ni	-0.62	-0.55
Si	0.44	0.81
Total:	100	100

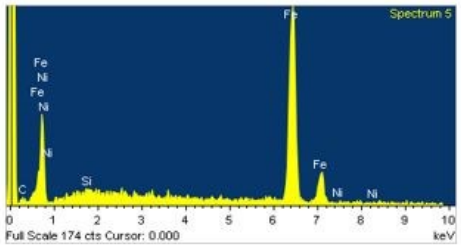

Figure 24: Chemistry, EDS spectrum, and area analysis of substrate of Sample #3, cast at Maynard Steel. JOEL SEM, 27x, WD 12mm, accelerating voltage of 15 keV.

4.4 Vickers Microhardness Results

Vickers microhardness testing is often used to analyze the differences in hardness between the surface and substrate of surface modified components. In this test, the applied load and resultant indentation size are small relative to the bulk tests, such as Brinell hardness testing. Here, the test material is indented with a pyramidal diamond indenter, with a specific dwell time and amount of force applied[39]. For these experiments, a 500 gf force with a dwell time of 10 seconds was used.

Ten surface measurements and ten substrate measurements were performed on each sample from Maynard Heat 2 and 3. For the surface measurements, three hardness tests were taken near the top surface, four were taken in the middle of the surface, and three were taken near the surface/substrate interface. For bulk measurements, three tests were taken just below the surface/substrate interface, four were taken near the middle of the substrate, and three were taken

at the bottom. Below are the surface and substrate microhardness results from Maynard Sample #7.

Maynard Sample 7 Surface

Position	HV_{500}
1	482
2	487
3	490
4	486
5	492
6	479
7	483
8	482
9	492
10	489
Average	486.2

Maynard Sample 7 Substrate

Position	HV_{500}
1	148
2	159
3	158
4	152
5	149
6	153
7	158
8	149
9	155
10	153
Average	153.4

Figure 25: Microhardness averages of Maynard Sample #7

The results indicate that the average surface hardness is approximately 3.17 times higher than the substrate hardness. These results show that the hardness increased as the alloying elements were melted and solidified onto the surface of the casting. This could possibly be due to the alloying elements acting as a chill when coming in contact with the molten metal during casting, and solidifying rapidly near the interface, causing there to be in increase in hardness.

4.5 X-Ray Diffraction Results

X-Ray Diffraction (XRD) is an important tool used to characterize the phases present in metallic specimens. This analytical test involves using x-rays to impinge a solid material surface, in which a portion of the beam will be scattered by the electrons associated with each atom that lies within the beam's path. The diffraction occurs when each object in a periodic array scatters the radiation coherently, producing constructive interference at specific angles[40]. The electrons in the sample coherently scatter the light, and the wavelength of x-rays are similar to the distance

between atoms. The diffraction of different planes of atoms produce different x-ray diffraction patterns, which ultimately gives information about the atomic arrangement within a crystal. This tool is useful to this study to investigate the various crystal phases present in the surface of the material, and compare that to the crystal phases present in the substrate[41].

Samples from the third heat at Maynard were studied using XRD, and the results are shown below. The XRD peaks for the substrate and for the surface were compared against known XRD peaks for CF3 stainless steel and WCB plain-carbon steel, to see if the peaks had similar expected phases to these materials.

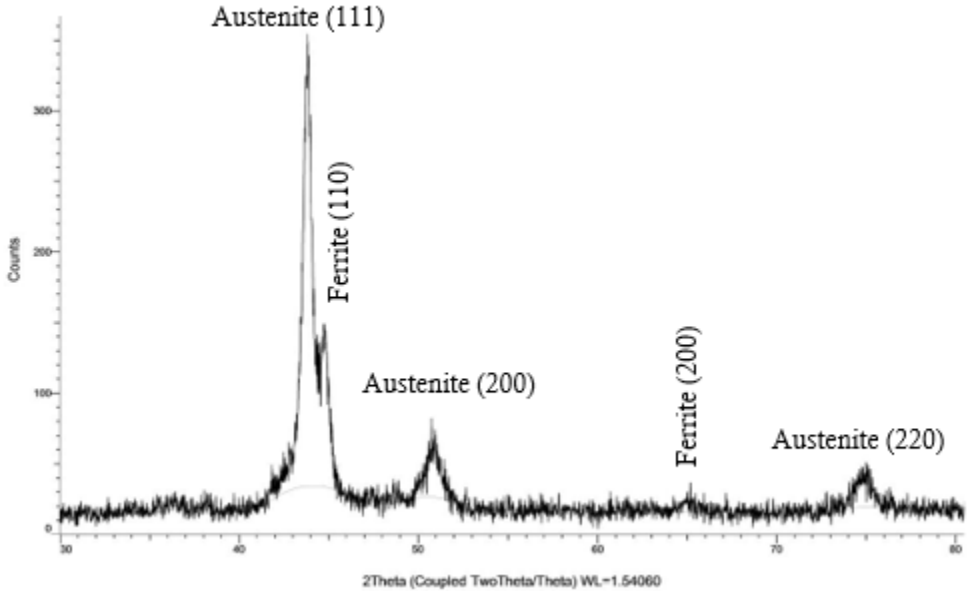

Figure 26: The XRD peaks for the surface of Maynard Sample #7.

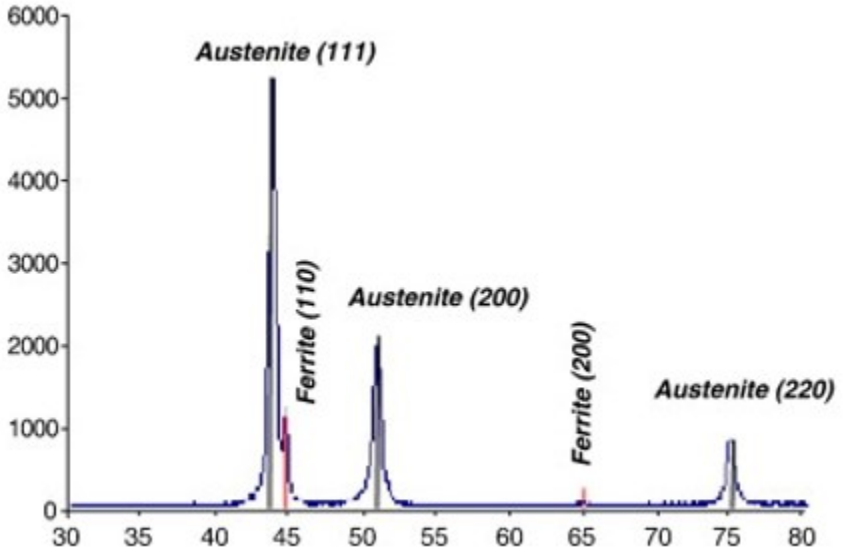

Figure 27: The XRD peaks for the surface of CF3 stainless steel alloy[42].

The peaks for the surface of Maynard Sample #7 show the presence of austenite and ferrite. Austenite has peak intensities near 43°, 52°, and 75°, while ferrite has peak intensities near 44° and 65°. When compared to the known XRD peaks for CF3 stainless steel[41], it is clear that the peaks from Sample #7 are in the same locations, indicating the surface having a crystal structure primarily of austenite and ferrite. This is to be expected, since nickel is a known austenite stabilizer, and chromium is a ferrite stabilizer. CF3 is an austenitic stainless steel, and the results of the XRD show that the phases on the surface of Maynard Sample #7 are the same as a CF3 cast alloy.

The substrate was also analyzed using XRD to determine if it had the expected crystal structure of non-heat treated WCB steel, which would be possess a ferritic crystal structure. Below are the XRD peaks for the substrate of Sample #7.

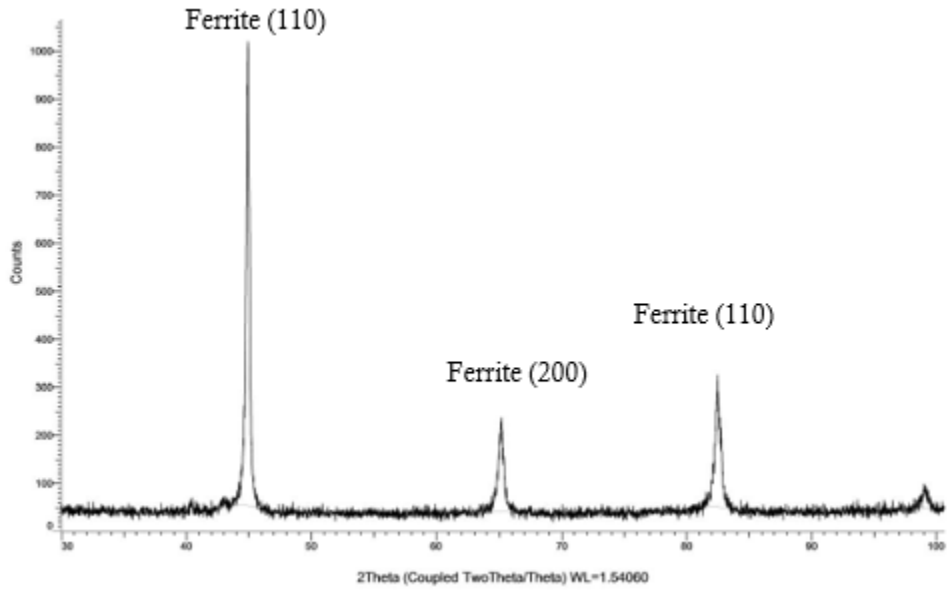

Figure 28: The XRD peaks for the substrate of Maynard Sample #7

The peaks indicate a presence of ferrite in the bulk of Sample #7. There is no presence of austenite, which shows that the nickel did not diffuse into the substrate layer, and that the bulk of the material is entirely plain-carbon steel. The patterns for the surface and the patterns for the substrate of Maynard Sample #7 show that there are different crystal structures on the same sample, and that they correspond with the known peaks for CF3 and WCB[43], proving that the surface enrichment only on the surface occurred during casting.

4.6 Linear Polarization Test Results

Linear polarization testing was used to measure the corrosion current of the surface of the sample and for the bulk of the sample. The material is polarized during this test on the order of +/- 10 mV on an open circuit potential[43], and the potential is measured when no net current is flowing. As the potential of the working electrode is changed, a current will be inducted to flow between the working and counter electrodes, and the sample's resistance to polarization is found by taking the slope of the potential vs current curve[44].

Maynard Samples # 7, 8, and 9, as well as the substrate material, were analyzed using a linear polarization test. With the help of Dr. Bob Bauer, the samples were conditioned in an ASTM G61 3.56% salt water solution[45] for one hour, and then underwent a linear polarization test for 10 minutes. After the test was completed, the corrosion current was extrapolated from the results of the experiment, and were then used to calculate the corrosion rate. The results of the linear polarization test for the substrate of Maynard Sample #7, and for the surface of the same sample, are given below.

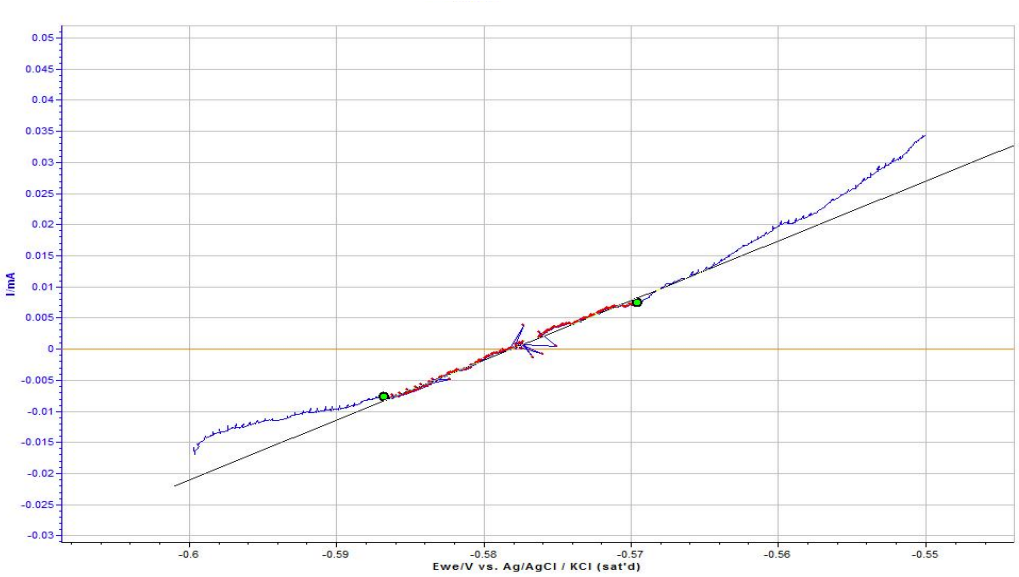

Figure 29: The linear polarization results for the substrate of Maynard Sample #7

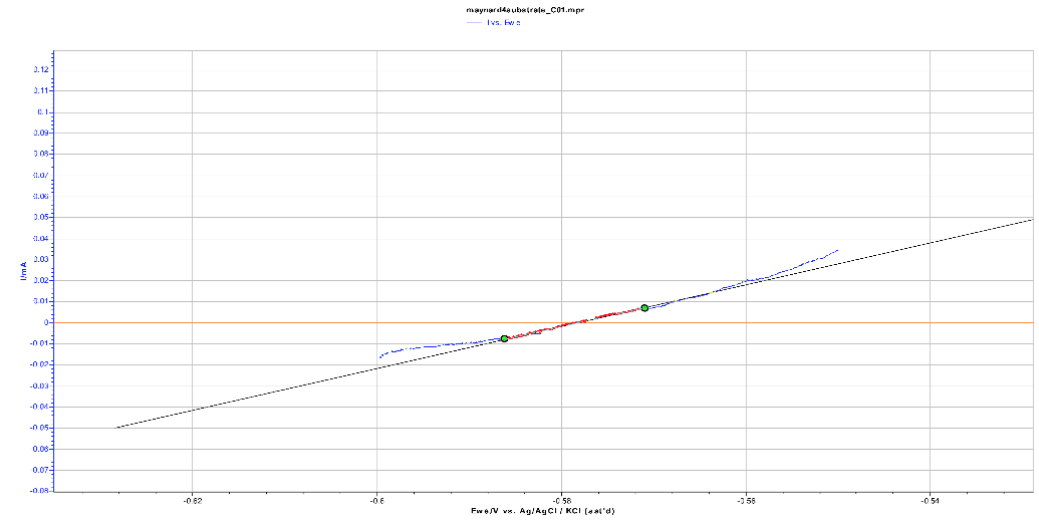

Figure 30: The linear polarization results for the surface of Maynard Sample #7

The corrosion current was calculated to be 25.45 μA for Maynard Sample #7 steel substrate, and 4.31 μA for the enriched surface of the same sample, after the linear polarization tests were completed. To calculate the corrosion rate, the corrosion current must be changed to the corrosion current density, using the following equation[46]

$$i_{cor} = \frac{I_{cor}}{A}$$

Where:

$$i_{cor} = corrosion\ current\ density, \frac{\mu A}{cm^2}$$
$$I_{cor} = total\ anodic\ current, \mu A$$
$$A = exposed\ specimen\ area, cm^2$$

The equivalent weight is also needed to calculate the corrosion rate[47]. The equivalent weight for each element and alloy is different, and the equation which follows shows how to calculate equivalent weight for a pure material. The WCB equivalent weight was treated as a pure material, because it consists of over 99% iron[48].

$$EW = \frac{W}{n}$$

Where:

$$W = the\ atomic\ weight\ of\ the\ element$$
$$n = the\ valence\ of\ the\ element$$

For an alloy, the equivalent weight must total the equivalent weights of each metal in the system, and then must be added up and divided by 100. Below is the equation which details how to calculate equivalent weight of an alloy[49]

$$Q = \sum \frac{nifi}{Wi}$$

Where:

$$fi = the\ mass\ fraction\ of\ the\ i^{th}\ element\ in\ the\ alloy$$
$$Wi = the\ atomic\ weight\ of\ the\ i^{th}\ element\ in\ the\ alloy$$
$$ni = the\ valence\ of\ the\ i^{th}\ element\ in\ the\ alloy$$

The density of the material must also be considered to calculate corrosion rate. To find the density, the following equation must be applied

$$\rho = density\ in\ \frac{g}{cm^3}$$

After calculating the necessary components for the corrosion rate equation, they can be substituted back into the equation for corrosion rate, which is as follows[50]

$$CR = K_1 \frac{i_{cor}}{\rho} EW$$

Where:

$$CR\ is\ given\ in\ \frac{mm}{yr}, i_{cor}\ in\ \frac{\mu A}{cm^2}$$

$$K_1 = 3.27x10^{-3}\ \frac{mm\ g}{\mu A\ cm\ yr}$$

The corrosion rate of plain-carbon steel was determined to be 0.609 mm/yr, while the corrosion rate of Maynard Sample #7 was determined to be 0.066, indicating that the corrosion resistance of the surface is 10.8 times higher than the corrosion rate of the substrate. The same procedure was used to determine the corrosion rates of Maynard Samples #8-9 as well. The corrosion rate of Maynard Sample #8 was calculated as 0.071 mm/yr, and the corrosion rate of Maynard Sample #9 was calculated as 0.087 mm/yr. This indicates that the surfaces of the Maynard Samples enriched with nickel and chromium powder ranged from 10.8 – 14.0 times more corrosion resistance than the base steel.

5. Conclusions

The following conclusions can be drawn based off of the results generated during the experimentation for surface alloying as well as during the characterization testing. Figures 79 and 80, in Appendix B, summarize the results of the project as well.

1. The thickness of the enriched layers was measured with the optical microscopy software, and it was determined that for Maynard samples 3, 4, 5, and 6, enriched only with nickel, the thicknesses of the surface enriched layers ranged from an average of 1148 μm to 1584 μm. The thicknesses of the enriched layers for Maynard samples 7, 8, 9, and 10, enriched with nickel and chromium, ranged from an average of 297 μm to 352 μm. Although more material was used in the nickel and chromium coatings when compared to only nickel, the nickel and chromium layer measured thinner than the only nickel layer. This indicates that layer thickness is not dependent on amount of material used.
2. The EDS chemical analysis of the cross sections suggests that there is no significant composition gradient in either the coatings or the substrates. Below the surface/substrate interface, there is primarily WCB steel composition present, with no measurable alloying elements present. In the enriched surface layer, nickel and iron were present when only nickel powder was used, and nickel, chromium, and iron were present when the nickel and chromium powders were present in the slurry coatings on the mold.
3. The results of the Vickers microhardness test indicate that there is a substantial difference in microhardness between the enriched surface and the substrate. The substrate has microhardness values close to that of WCB steel, which is 155 HV500. The surfaces of the samples with enriched surfaces were much harder, ranging from 479-488 HV500. This harder layer could be caused by the rapid solidification during casting, and can provide better wear-resistant properties on the surface.
4. The results of the XRD illustrate the difference in crystal structures between the enriched surface layer and the base steel substrate. The location of the peaks for the enriched layer matched with austenite and ferrite structures, which would be expected in an austenitic stainless steel like CF3. The peaks for the steel substrate matched with only ferrite,

which is what would could be expected in non-heat treated WCB steel. The results of the XRD show that there are not only different crystal structures between the enriched surface and the steel substrate, but they are the crystal structures that would be expected for both stainless steel and plain-carbon steel, respectively.

5. The corrosion rates of the three Maynard Steel samples enriched with nickel and chromium ranged from 0.066 mm/yr to 0.087 mm/yr, respectively. When compared to the corrosion rate of WCB, which is 0.609 mm/yr, this shows that the corrosion resistance of the enriched surfaces were 10.8 – 14.0 higher than the base steel.

6. Future Work

The main focus of this study was to determine if a surface layer enriched in chromium and nickel could be formed through mold coating, and metallurgically bonded to a plain carbon steel substrate via a sand casting process. A novel and unique design of a slurry, which was tailored to adhere specifically to silica sand, was discovered over the course of the trials at Maynard Steel, as well as laboratory experiments at UWM. The slurry has been demonstrated to be effective in releasing the alloying elements onto the surface of the steel during casting, and upon solidification, there is a continuous, distinct layer that has chemistry similar to that of CF3 grade stainless steel. There are some factors, however, that should be taken into consideration when continuing on this work, as well as additional testing techniques that should be carried out.

The adhesion of the surface layer should be measured, and there are multiple techniques that are able to do so, such as the tape method, the pull-off test, the shock wave loading method, and the scratch test. The scratch test uses a chrome-steel stylus with a tungsten carbide or Rockwell C diamond tip, or can use a Vickers microhardness tester as well. Both of these testing techniques can be performed at UWM. According to Fahlman, to perform the scratch test, the

stylus is drawn across the surface of the coating, and a vertical load is applied and is increased until the coating is removed. The minimum critical load at which the coating fails or chips is used to measure the adhesion.

The use of this technology for making surfaces corrosion resistant for use in the water industry was the driving force behind this study. Since the surface that comes in contact with the water is the one that was alloyed, it must be implemented in the field as cast, and without machining. Therefore, it is in the best interest of future researchers to develop ways to achieve an excellent as-cast surface, which is smooth, free of porosity, and continuous throughout the surface of the entire component.

In addition to improving the as-cast surface quality, controlling the thickness of the alloyed layer is another major area of focus. It is evident from the EDS chemical analysis that there is no gradient between the surface and the substrate; just below the threshold between the surface and substrate, there is no presence of the alloying elements, just the plain-carbon steel. For future research, heat-treating the samples at different temperatures for different amounts of time could reveal a diffusion profile. Annealing and normalizing are common techniques that should be implemented to study the effects of diffusion, and to see if the alloying elements will diffuse further at different times.

References

1. ASTM Standard A216 (WCA, WCB, WCC) 2016 "Standard Specification for Steel Castings, Carbon, Suitable for Fusion Welding, for High-Temperature Service." ASTM International, West Conshohocken, PA.
2. "Casting Material: Carbon Steel WCB." Qingdao Casting Quality Industrial Co., Ltd., 2016.
3. Monroe, R. "Specifying Steel Castings." Steel Founders Society of America. Crystal Lake, Il, 2017.
4. ASTM Standard A351 "Specification Standard for Stainless Steel Casting." 2017, ASTM International, West Conshohocken, PA.
5. "Specification Sheet: Alloy 304/304L (UNS S30400, S30403)." Sandmeyer Steel Company, Philadelphia, PA, 2014.
6. Desu, R. "Mechanical properties of Austenitic Stainless Steel 304L and 316L at elevated temperatures." Journal of Materials Research and Technology, vol. 5, issue 1, 2016.
7. Hermas, A. "Microstructure, corrosion, and mechanical properties of 304 stainless steel containing copper, silicon, and nitrogen." Journal of Materials Science, p. 3415-3421, 2001.
8. Baldenebro, F. Gomez-Esparza, C. "Influence of Size on Microstructure and Mechanical Properties of an AISI 304L Stainless Steel- A Comparison between Bulk and Fibers." Materials, p. 451-461, 2015.
9. Lorang, G. "Chemical Composition of Passive Films on AISI 304 Stainless Steel." Journal of The Electrochemical Society, vol. 141, issue 12, 1994.
10. Aramide, F. Ibitoye, S. "Effects of carburization time and temperature on the mechanical properties of carburized mild steel, using activated carbon as carburizer." Materials Research, vol. 12, no. 4, 2009.
11. S. S. Hosmani et al., "An Introduction to Surface Alloying of Metals." Springer Briefs in Manufacturing and Surface Engineering, 2014.
12. Koerner, H. Landes, H. "The effect of carburization and oxygen exposure on the reaction of carbon monoxide on iron films at 573K under a pressure between 5 and 10 mbar." Applications of Surface Science, vol. 18, Issue 4, 1984.
13. Kannatey-Asibu Jr, Elijah. 'Principles of laser materials processing." Vol. 4, John Wiley & Sons, 2009.
14. Biswas, A. Maity, TK. Chatterjee, UK. "Trends in Biomaterials and Artificial Organs." MedIND, India, vol. 20, p. 68-71, 2006.
15. Niinomi, M, Liu, Y. "Biomedical titanium alloys with Young's moduli close to that of cortical bone." Regenerative Biomaterials, vol. 3, p. 173-185, 2016.
16. Meletis, E. Cooper, C. "Intensified plasma-assisted nitriding of AISI 316L stainless steel." Surface and Coatings Technology, vol. 160, Issue 2-3, 2002.
17. Yiming, C, Guochao, G. "Laser surface alloying on aluminum and its alloys: A review." Optics and Lasers in Engineering, vol. 100, p. 23-37, 2017.
18. Sarkar, S. Raj, M. "Transport phenomena in laser surface alloying." Journal of Materials Science, vol. 38, Issue 1, p. 155-164, 2003.
19. Draper, CW. Ewing, CA. 'Laser surface alloying- a bibliography." Journal of Materials Science, vol. 19, Issue 12, 1984.
20. Pelletier, J. Issa, A. Fouquet, F. "Possibilities and Limitations of Laser Surface Alloying

by Melting of Predeposited Layers." Journal de Physique IV Colloque, p. 87-90, 1991.
21. Fatoba, O. Popoola, P. "Computational Dynamics of Anti-Corrosion Performance of Laser Alloyed Metallic Materials." Fiber Laser, 2016.
22. Das, DK. "Evolution of microstructure in laser surface alloying of aluminum with nickel." Materials Science and Engineering: A, vol. 174, Issue 1, p. 75-84, 1994.
23. Rhodes, C. Mahoney, M. Bingel, W. "Effect of friction stir welding on microstructure of 7075 aluminum." Scripta Materialia, p. 69, 1997.
24. Fujii, H. Sun, Y. Kato, H. "Microstructure and mechanical properties of friction stir welded pure Mo joints." Scrupta Materialia, vol. 64, Issue 7, p. 657-660, 2011.
25. Friction Stir Welding, Universite du Quebec a Chicoutimi, http://www.uqac.ca/ceeuqac.
26. Miracle, DB. "Metal matrix composites- from science to technological significance." Composites Science and Technology, vol. 65, Issue 15-16, p. 2526-2540, 2005.
27. Mishra, RS. Ma, Z. "Friction stir processing: a novel technique for fabrication of surface composite." Materials Science and Engineering: A., vol. 341, Issues 1-2, p. 307-310, 2003.
28. Mahoney, M. Mishra, R. Nelson, T. "TMS proceedings, friction stir welding and processing." Materials Science and Engineering, p. 183-194, 2001.
29. Mahmoud, E. Ikeuchi, K. "Fabrication of SiC particle reinforced composite on an aluminum surface by friction stir processing." Science and Technological Welding and Joining, 2008.
30. Baba, K. Hatada, R. "Proceedings of DAE-BRNS workshop on plasma surface engineering." Applied Publishers, Ltd, p. 28-44, 2004.
31. Mukherjee, S. "Proceedings of DAE-BRNS workshop on plasma surface engineering." Applied Publishers, Ltd, p. 181-199, 2004.
32. Shim, Y. Kim, Y. Lee, K. "The properties of AlN prepared by plasma nitriding and plasma source ion implantation techniques." Surface and Coatings Technology, vol. 131, Issues 1-3, 2000.
33. Sioshansi, P. Tobin, EJ. "Surface treatment of biomaterials by ion beam process." Surface and Coatings Technology, vol. 83, Issues 1-3, p. 175-182, 1996.
34. Hasan, MF. "Analysis of Mechanical Behavior and Microstructural Characteristics Change of ASTM A-36 Steel Applying Various Heat Treatment." Journal of Materials Science and Engineering, vol. 5, 201.
35. Rosenberg, S. Darr, J. "Stabilization of Austenitic Stainless Steel." U.S. Department of Commerce, National Bureau of Standards. Vol. 40, 1948.
36. Chalker, P.R., Bull, S.J. "A review of the methods for the evaluation of coating-substrate adhesion." Materials Science and Engineering: A, vol. 140, p. 583-592.
37. Callister, W., Rethwisch, D. "Materials Science and Engineering An Introduction." Edition 8, John Wiley & Sons, Inc., p. 111.
38. Yacobi, B.G., Kazmerski, L.L., Holt, D.B. "Microanalysis of Solids, Scanning Electron Microscopy." Springer Science, p. 25-27, 1994.
39. Mohrnheim, A. "Microhardness Testing and Hardness Numbers." Interpretive Techniques for Microstructural Analysis, Springer, Boston, MA, 1997.
40. Tiwari, A. Turner, A. "Biosensors Nanotechnology." Scrivener Publishing, Wiley, p. 18-19, 2014.
41. Chipera, S. Bish, D. "Fitting Full X-Ray Diffraction Patterns for Quantitative Analysis:

A Method for Readily Quantifying Crystalline and Disordered Phases." Advances in Materials Physics and Chemistry, vol. 3, p. 47-53, 2013.

42. Olaseinde, W. Van der Merwe, J. "Characterization and Corrosion Behaviour of Selected Duplex Stainless Steels in Acidic and Acid-Chloride Solution." Advances in Chemical Engineering and Science, vol. 4, No. 1, 2014.

43. "Linear Polarization Resistance and Corrosion Rate, Theory and Background." Pine Research, Rev 002, April 2016.

44. "ASTM Standard Practice for Calculation of Corrosion Rates and Related Information from Electrochemical Measurements." ASTM International, West Conshohocken, PA, 2002.

45. "ASTM Standard Test Method for Conducting Cyclic Potentiodynamic Polarization Measurements for Localized Corrosion Susceptibility of Iron-, Nickel-, or Cobalt-Based Alloys." ASTM International, West Conshohocken, PA, Book of Standards vol. 03.02.

46. Dean, S.W. "Materials Performance." vol. 26, p. 51-52, 1987.

47. Pourbaix, M. "Atlas of Electrochemical Equilibrium in Aqueous Solutions." National Association of Corrosion Engineers, Houston, TX, 1974.

48. Sherif, E.S. "A Comparative Study on the Electrochemical Corrosion Behavior of Iron and X-65 Steel in 4.0 wt% Sodium Chloride Solution after Different Exposure Intervals." Molecules Open Access, 2014.

49. Silverman, D.C. "Corrosion." Vol. 37, p. 546-548, 1981.

50. Dean, S.W., France, W.D. "Electrochemical Methods for Corrosion Testing." Electrochemical Techniques for Corrosion, National Association of Corrosion Engineers, Houston, TX< p. 52-53, 1977.

Appendix A

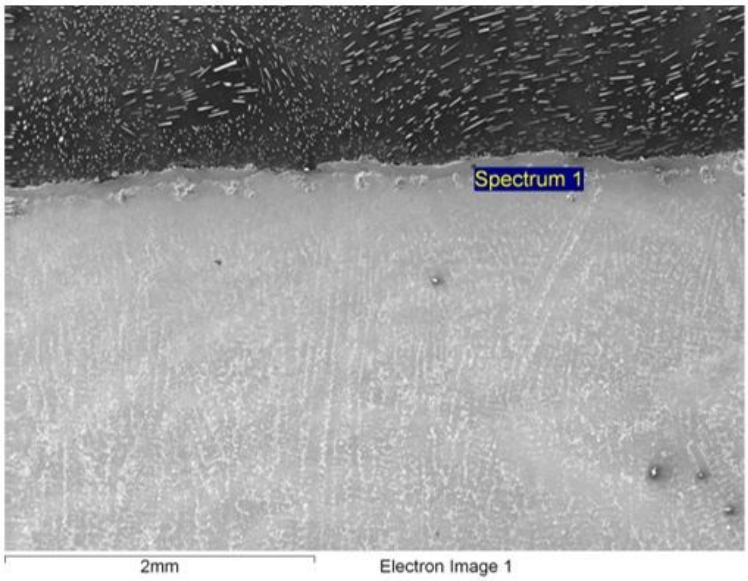

Sample #1

Element	Weight %	Atomic %
Fe	97.67	95.83
Ni	0.02	0.11
Si	1.99	3.81
Cu	0.34	0.29
Total:	100.02	100.04

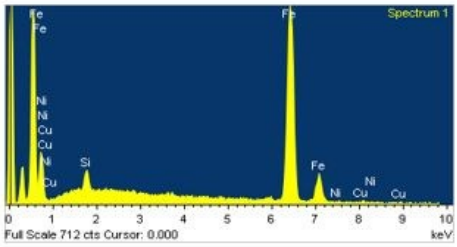

Figure 30: Chemistry, EDS spectrum, and point analysis of surface of Maynard Sample #1, cast at Maynard Steel. JOEL SEM, 27x, WD 12mm, accelerating voltage of 15 keV.

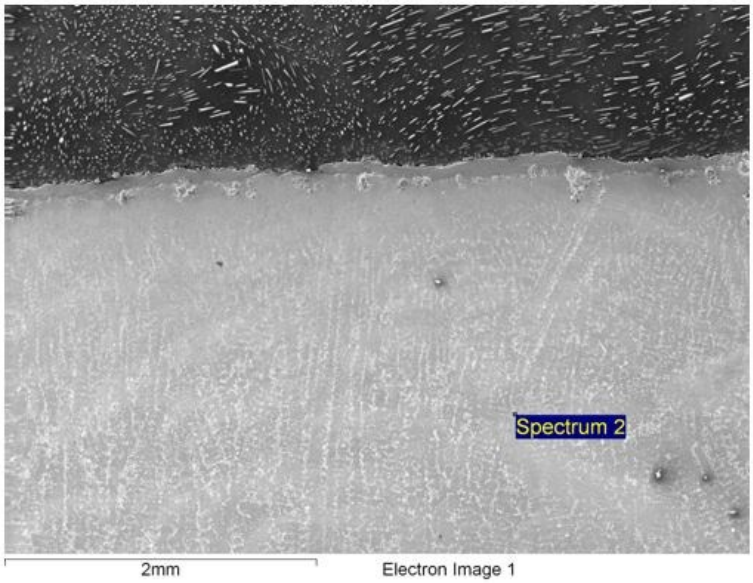

Sample #1

Element	Weight %	Atomic %
Fe	98.90	98.43
Ni	0.02	0.02
Si	0.55	1.09
Cu	0.53	0.47
Total:	100	100

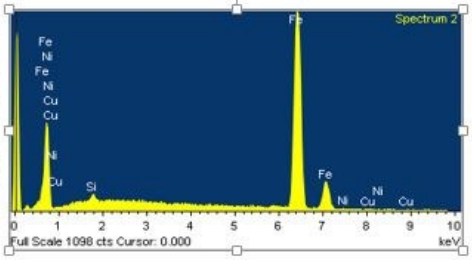

Figure 31: Chemistry, EDS spectrum, and point analysis of substrate of Maynard Sample #1, cast at Maynard Steel. JOEL SEM, 27x, WD 12mm, accelerating voltage of 15 keV.

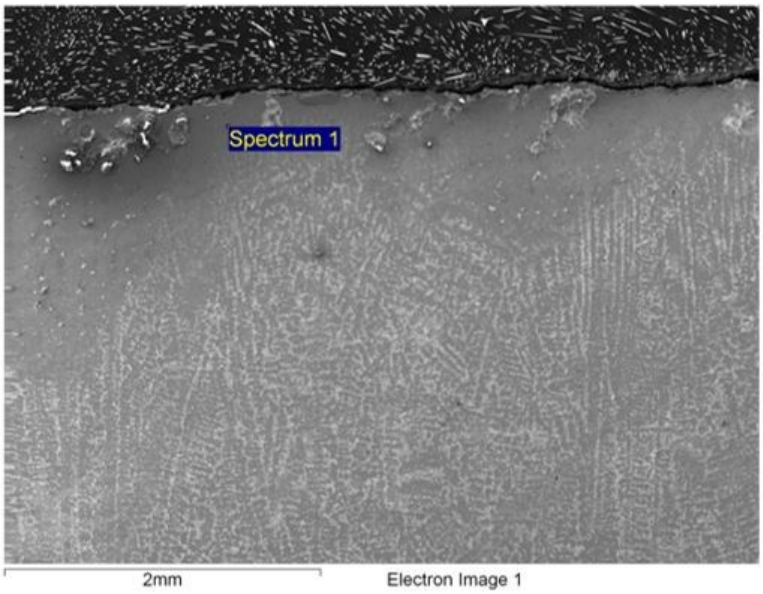

Sample #2

Element	Weight %	Atomic %
Fe	99.62	99.65
Ni	0.20	0.19
Cu	0.18	0.16
Total:	100	100

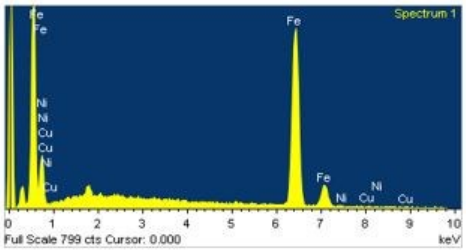

Figure 32: Chemistry, EDS spectrum, and point analysis of surface of Maynard Sample #2, cast at Maynard Steel. JOEL SEM, 27x, WD 12mm, accelerating voltage of 15 keV.

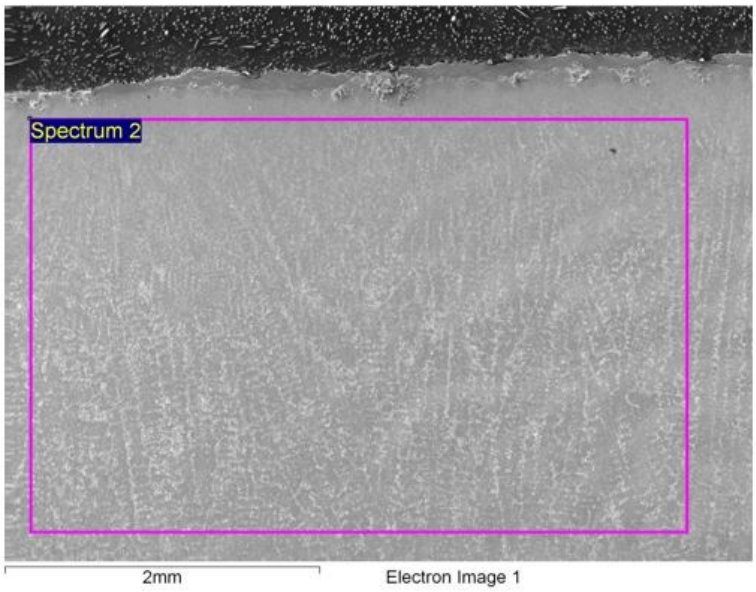

Sample #2

Element	Weight %	Atomic %
Fe	99.48	99.53
Ni	0.18	0.18
Cu	0.33	0.29
Total:	99	100

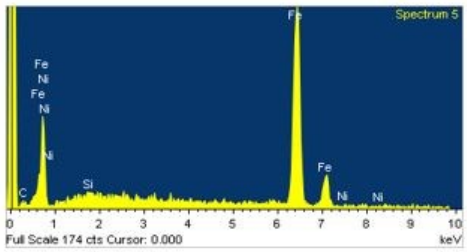

Figure 33: Chemistry, EDS spectrum, and area analysis of substrate of Maynard Sample #2, cast at Maynard Steel. JOEL SEM, 27x, WD 12mm, accelerating voltage of 15 keV.

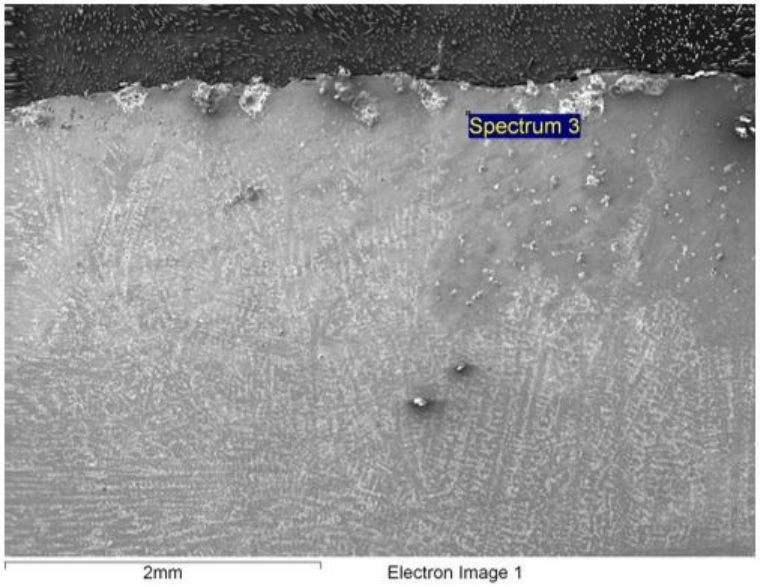

Sample #1

Element	Weight %	Atomic %
Fe	99.27	99.36
Ni	0.04	0.04
Cu	0.69	0.61
Total:	100	99

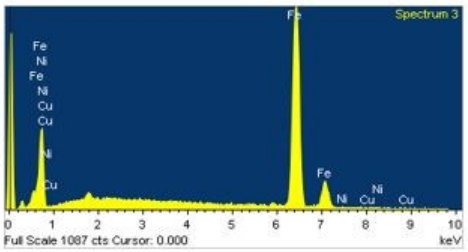

Figure 34: Chemistry, EDS spectrum, and point analysis of surface of UWM Sample #1, cast at UWM. JOEL SEM, 27x, WD 12mm, accelerating voltage of 15 keV.

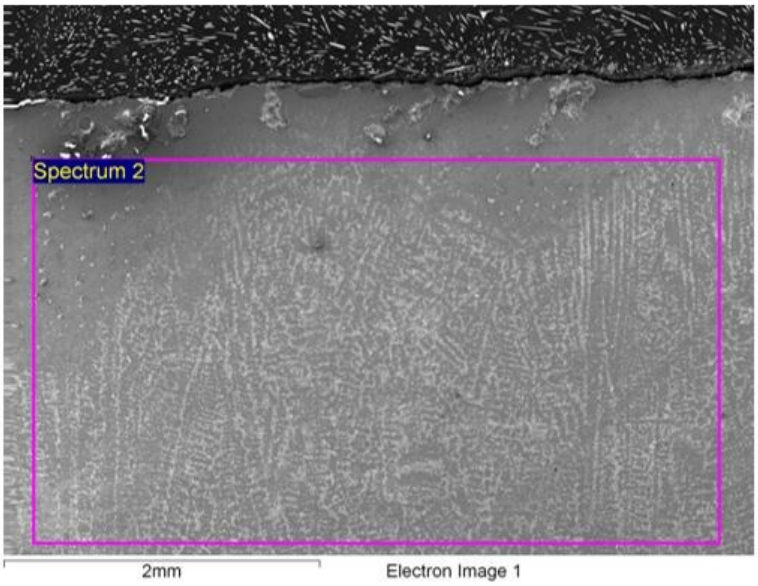

Sample #1

Element	Weight %	Atomic %
Fe	99.59	99.53
Ni	0.16	0.18
Cu	0.25	0.29
Total:	100	100

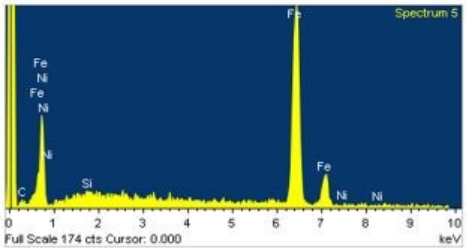

Figure 35: Chemistry, EDS spectrum, and area analysis of substrate of UWM Sample #1, cast at Maynard Steel. JOEL SEM, 27x, WD 12mm, accelerating voltage of 15 keV.

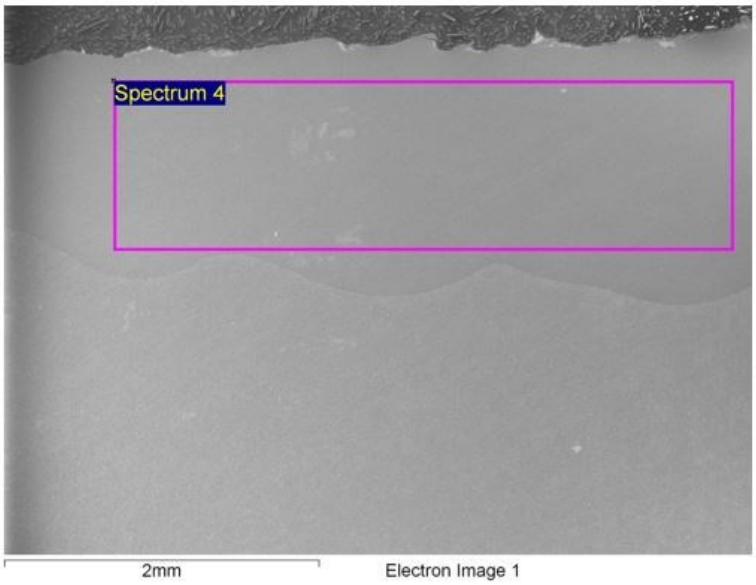

Sample #2

Element	Weight %	Atomic %
Fe	99.58	99.36
Ni	0.02	0.04
Cu	0.40	0.60
Total:	100	100

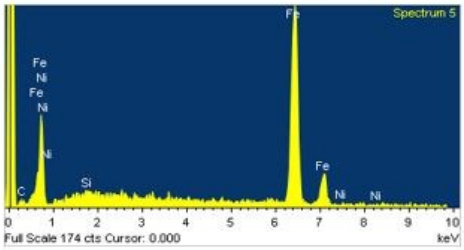

Figure 36: Chemistry, EDS spectrum, and point analysis of surface of UWM Sample #2, cast at UWM. JOEL SEM, 27x, WD 12mm, accelerating voltage of 15 keV.

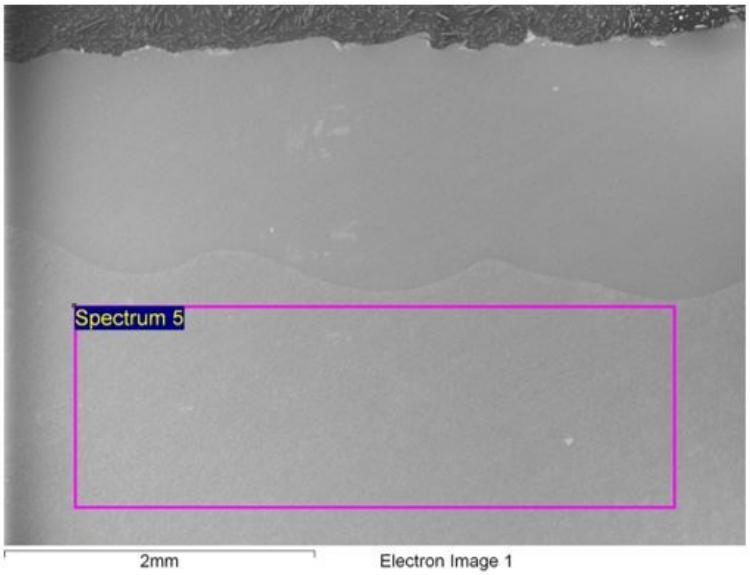

Sample #2

Element	Weight %	Atomic %
Fe	98.34	98.48
Ni	0.80	0.76
Cu	0.87	0.76
Total:	100	100

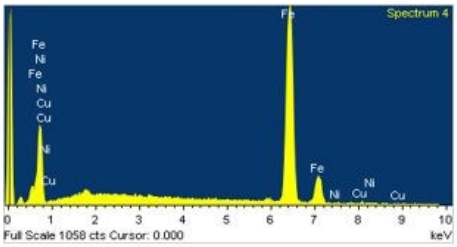

Figure 37: Chemistry, EDS spectrum, and area analysis of substrate of UWM Sample #2, cast at UWM. JOEL SEM, 27x, WD 12mm, accelerating voltage of 15 keV.

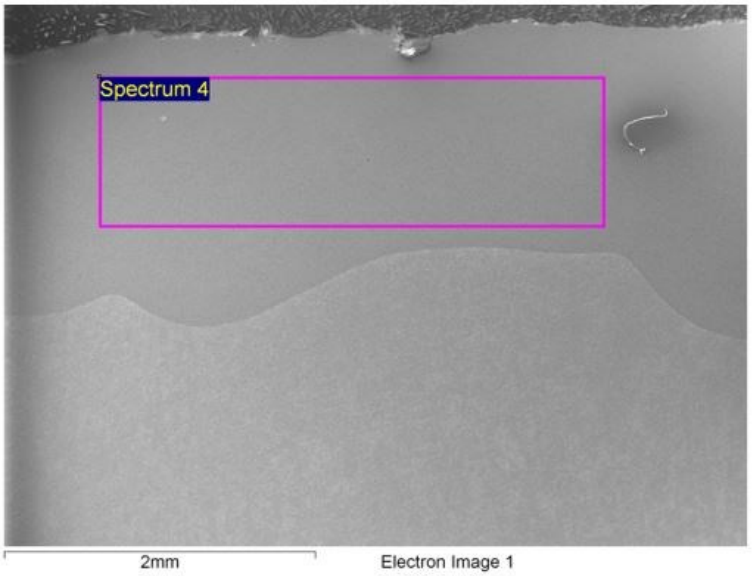

Sample #3

Element	Weight %	Atomic %
Fe	83.23	84.68
Ni	16.32	14.49
Si	0.45	0.83
Total:	100	100

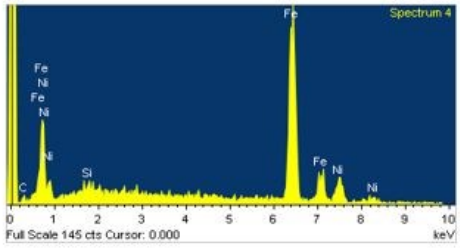

Figure 38: Chemistry, EDS spectrum, and area analysis of surface of Sample #3, cast at Maynard Steel. JOEL SEM, 27x, WD 12mm, accelerating voltage of 15 keV.

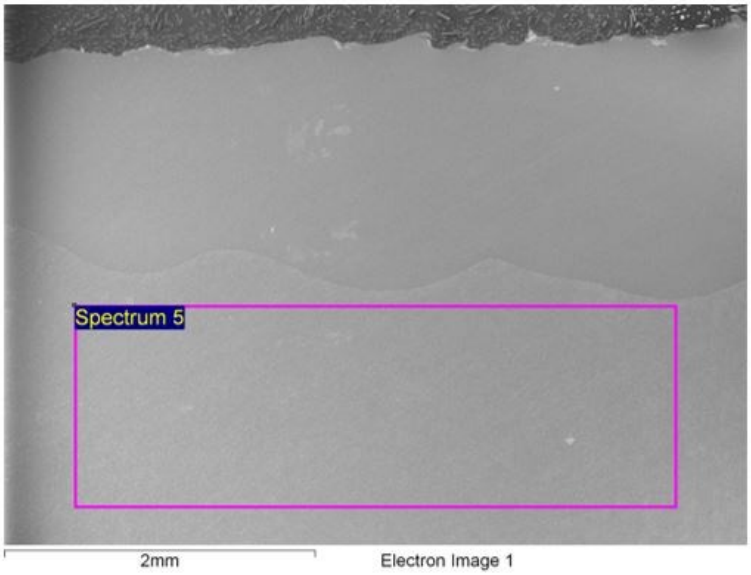

Sample #3

Element	Weight %	Atomic %
Fe	99.82	99.74
Ni	-0.62	-0.55
Si	0.44	0.81
Total:	100	100

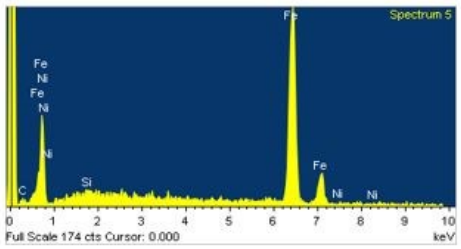

Figure 39: Chemistry, EDS spectrum, and area analysis of substrate of Sample #3, cast at Maynard Steel. JOEL SEM, 27x, WD 12mm, accelerating voltage of 15 keV.

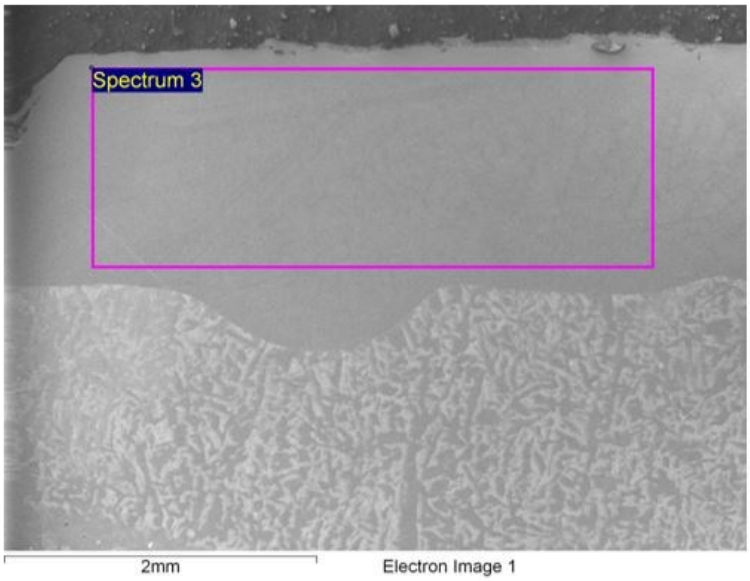

Sample #4

Element	Weight %	Atomic %
Fe	78.56	80.67
Ni	20.95	18.44
Si	0.48	0.89
Total:	99.9	100

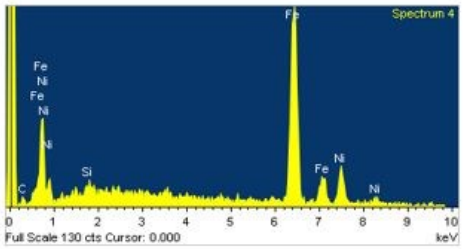

Figure 40: Chemistry, EDS spectrum, and area analysis of surface of Sample #4, cast at Maynard Steel. JOEL SEM, 27x, WD 12mm, accelerating voltage of 15 keV.

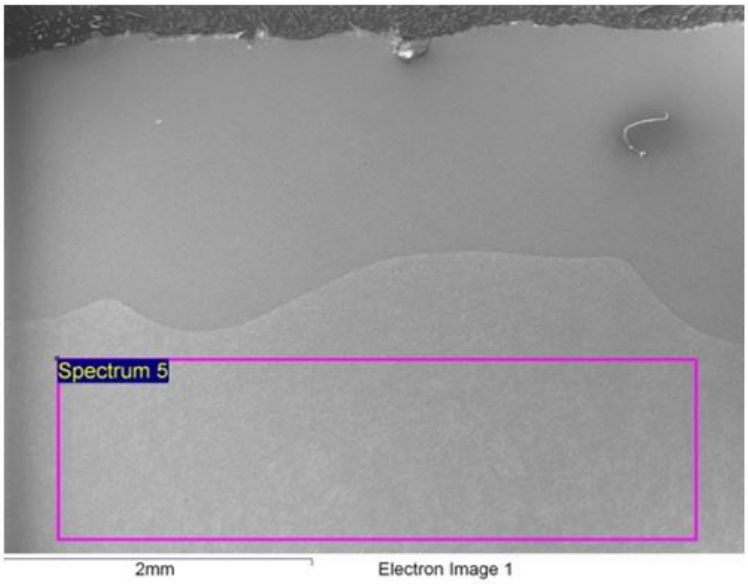

Sample #4

Element	Weight %	Atomic %
Fe	98.18	97.95
Ni	1.28	1.09
Si	0.54	0.96
Total:	100	100

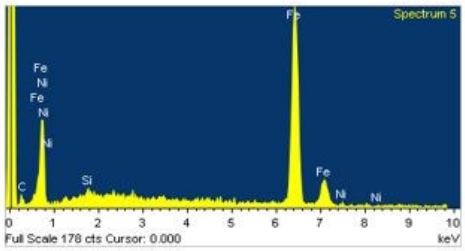

Figure 41: Chemistry, EDS spectrum, and area analysis of substrate of Sample #4, cast at Maynard Steel. JOEL SEM, 27x, WD 12mm, accelerating voltage of 15 keV.

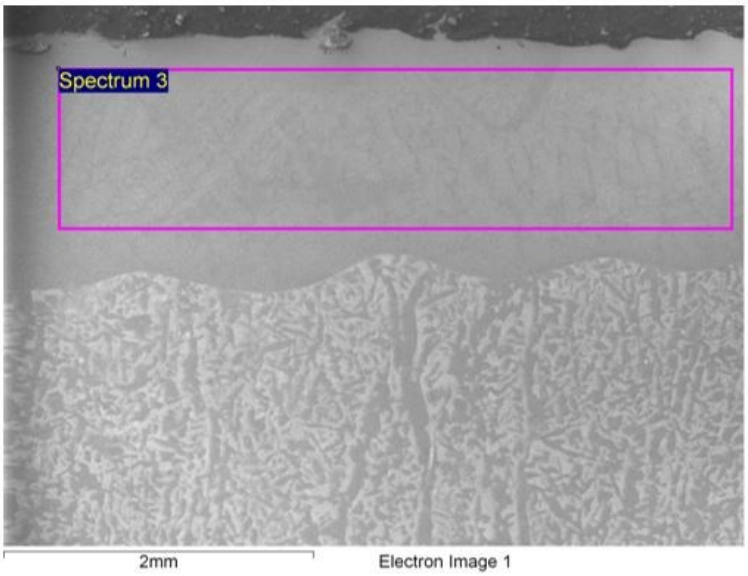

Sample #5

Element	Weight %	Atomic %
Fe	82.99	85.11
Ni	16.95	14.78
Si	0.06	0.11
Total:	100	100

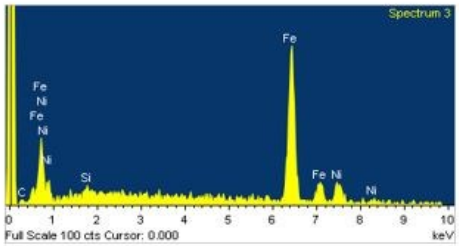

Figure 42: Chemistry, EDS spectrum, and area analysis of surface of Sample #5, cast at Maynard Steel. JOEL SEM, 27x, WD 12mm, accelerating voltage of 15 keV.

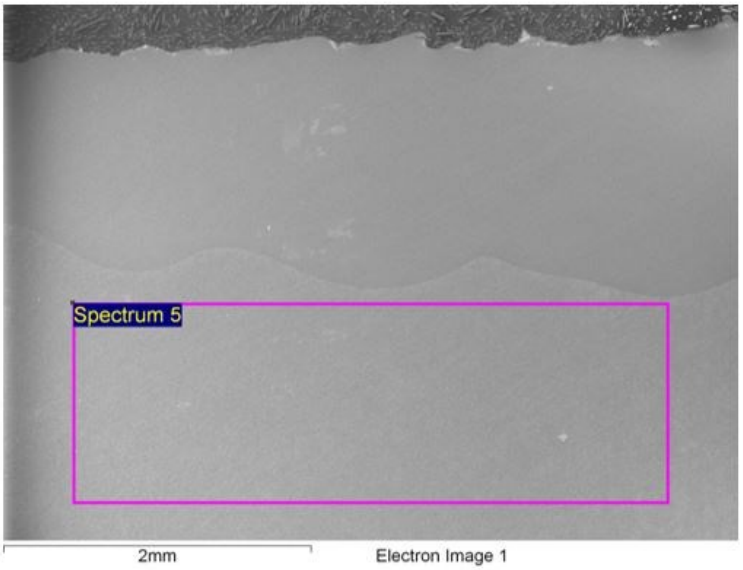

Sample #5

Element	Weight %	Atomic %
Fe	98.75	98.36
Ni	0.66	0.57
Si	0.59	1.07
Total:	100	100

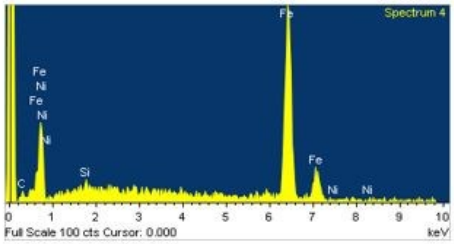

Figure 43: Chemistry, EDS spectrum, and area analysis of substrate of Sample #5, cast at Maynard Steel. JOEL SEM, 27x, WD 12mm, accelerating voltage of 15 keV.

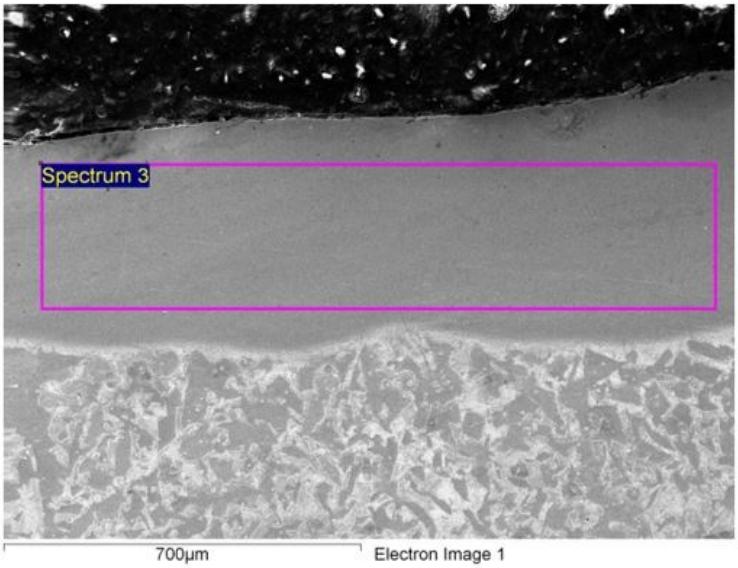

Sample #6

Element	Weight %	Atomic %
Fe	83.40	84.87
Ni	16.15	14.30
Si	0.45	0.84
Total:	100	100

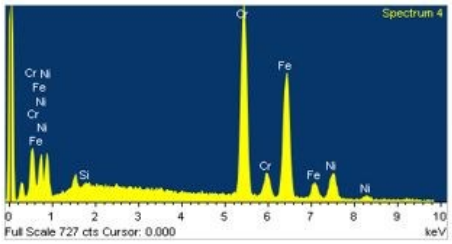

Figure 44: Chemistry, EDS spectrum, and area analysis of surface of Sample #6, cast at Maynard Steel. JOEL SEM, 27x, WD 12mm, accelerating voltage of 15 keV.

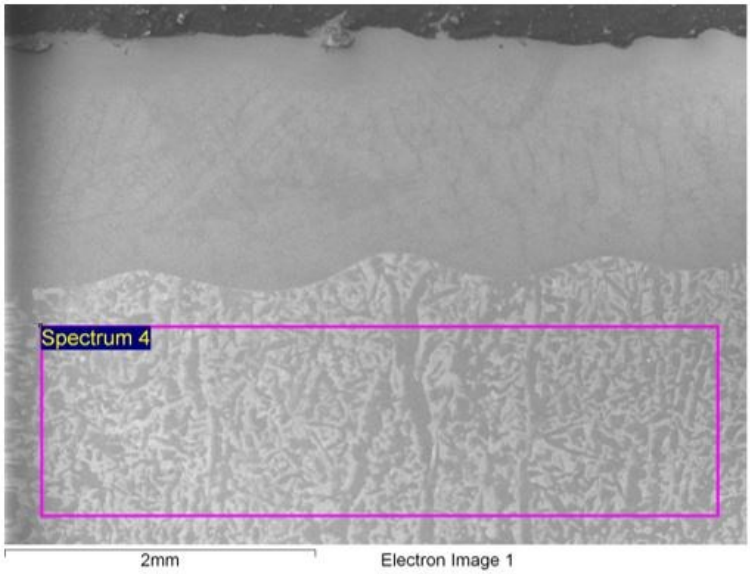

Sample #6

Element	Weight %	Atomic %
Fe	99.25	99.17
Ni	0.18	0.13
Si	0.57	0.70
Total:	100	100

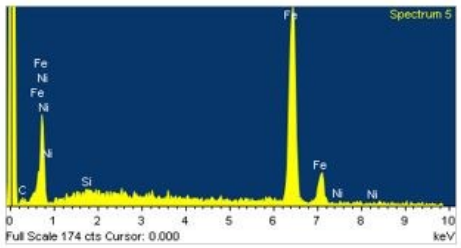

Figure 45: Chemistry, EDS spectrum, and area analysis of substrate of Sample #6, cast at Maynard Steel. JOEL SEM, 27x, WD 12mm, accelerating voltage of 15 keV.

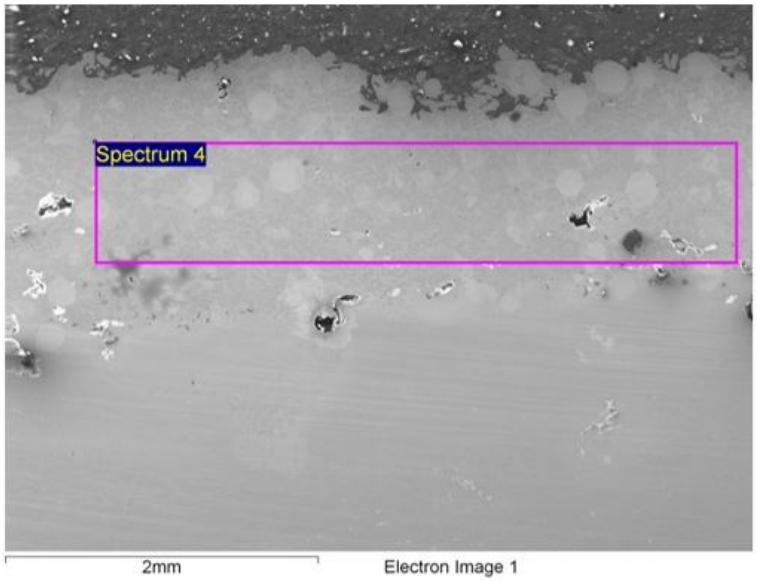

Sample #3

Element	Weight %	Atomic %
Fe	45.06	44.23
Ni	15.63	14.52
Cr	39.31	41.25
Total:	100	100

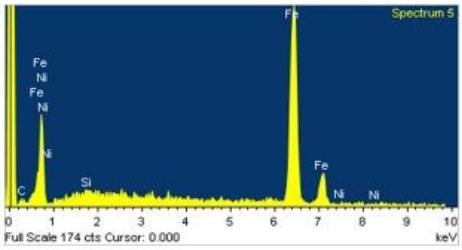

Figure 46: Chemistry, EDS spectrum, and area analysis of surface of UWM Sample #3, cast at Maynard Steel. JOEL SEM, 27x, WD 12mm, accelerating voltage of 15 keV.

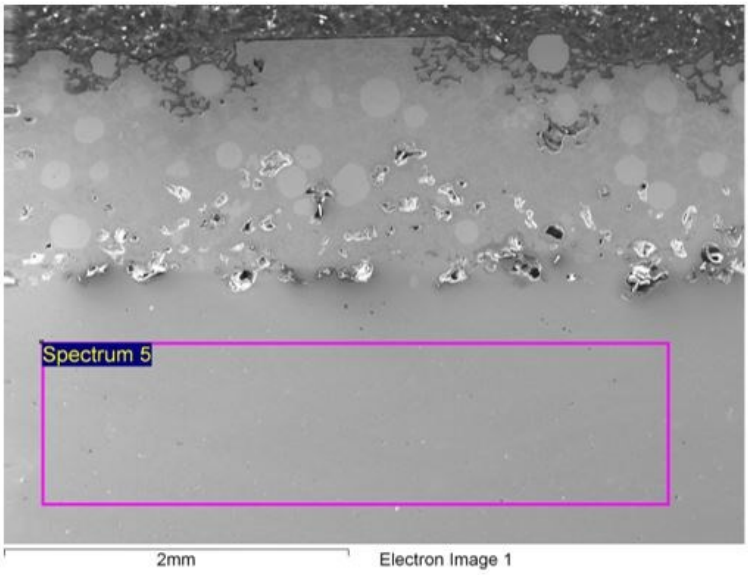

Sample #3

Element	Weight %	Atomic %
Fe	99.73	99.73
Ni	0.12	0.11
Cr	0.15	0.16
Total:	100	100

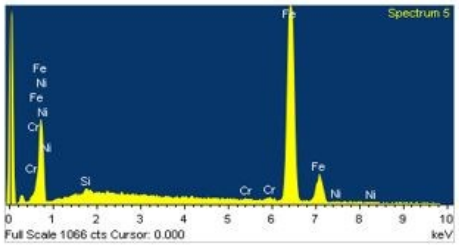

Figure 47: Chemistry, EDS spectrum, and area analysis of substrate of UWM Sample #3, cast at Maynard Steel. JOEL SEM, 27x, WD 12mm, accelerating voltage of 15 keV.

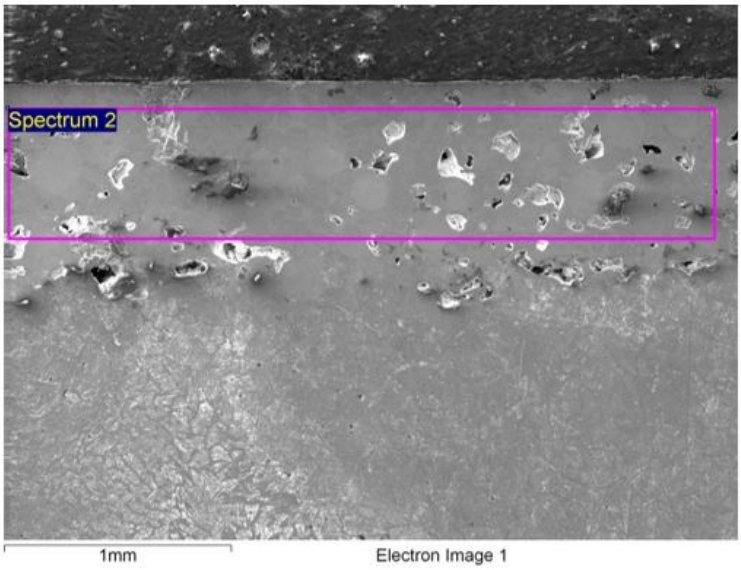

Sample #4

Element	Weight %	Atomic %
Fe	47.04	46.20
Ni	14.24	13.22
Cr	38.71	40.58
Total:	100	100

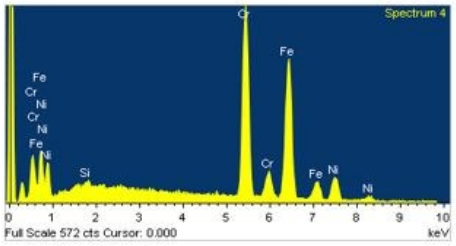

Figure 48: Chemistry, EDS spectrum, and area analysis of surface of UWM Sample #4, cast at Maynard Steel. JOEL SEM, 27x, WD 12mm, accelerating voltage of 15 keV.

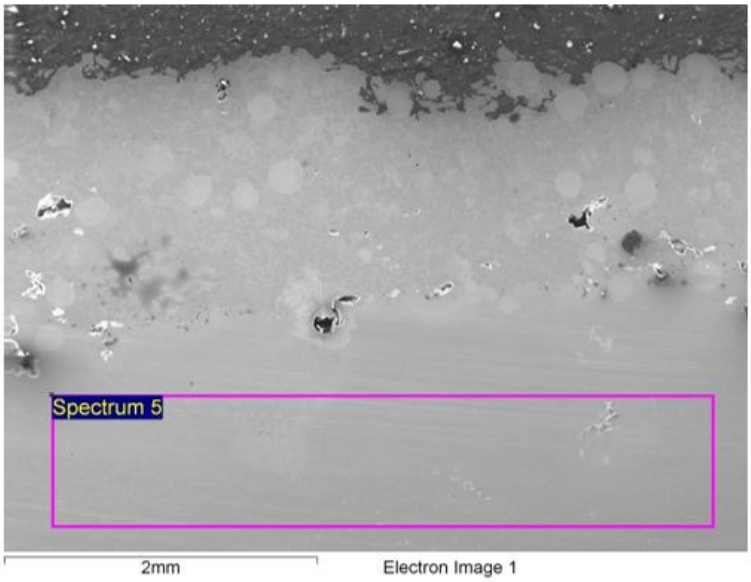

Sample #4

Element	Weight %	Atomic %
Fe	99.82	99.83
Ni	0.16	0.15
Cr	0.02	0.02
Total:	100	100

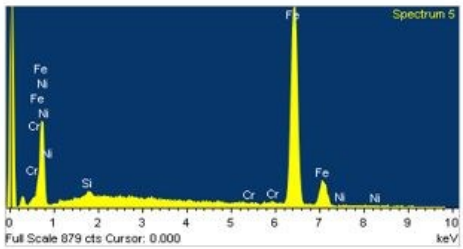

Figure 49: Chemistry, EDS spectrum, and area analysis of substrate of UWM Sample #4, cast at Maynard Steel. JOEL SEM, 27x, WD 12mm, accelerating voltage of 15 keV.

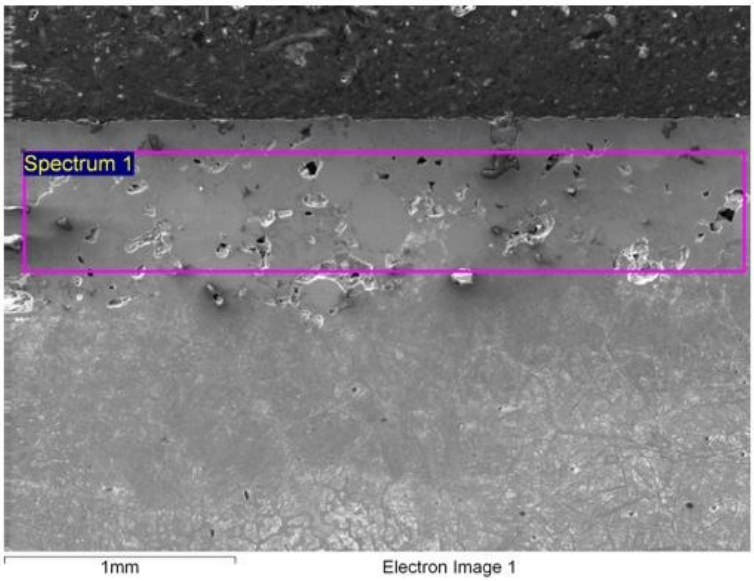

Sample #5

Element	Weight %	Atomic %
Fe	47.00	57.61
Ni	13.30	9.70
Cr	39.70	32.69
Total:	100	100

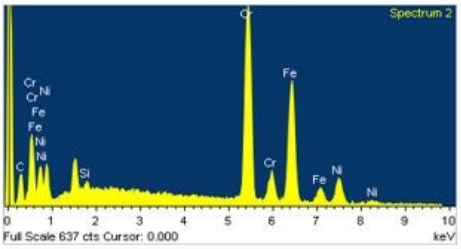

Figure 50: Chemistry, EDS spectrum, and area analysis of surface of UWM Sample #5, cast at Maynard Steel. JOEL SEM, 27x, WD 12mm, accelerating voltage of 15 keV.

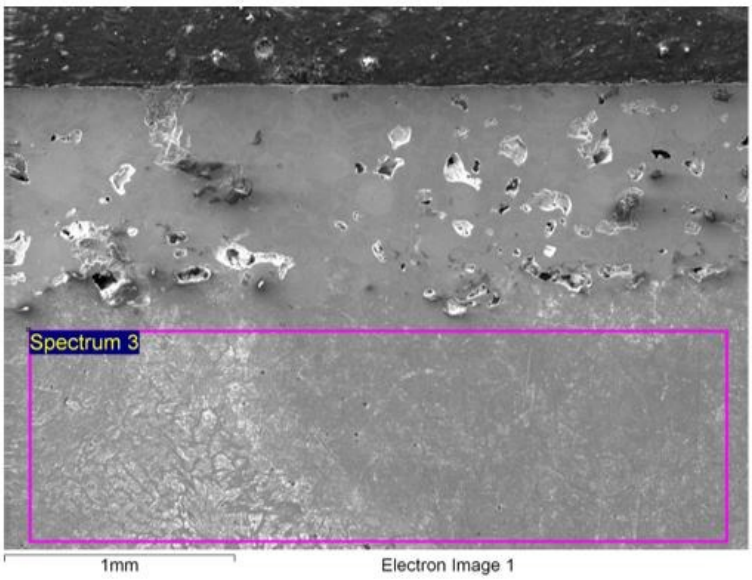

Sample #5

Element	Weight %	Atomic %
Fe	99.73	99.71
Ni	0.04	0.04
Cr	0.23	0.25
Total:	100	100

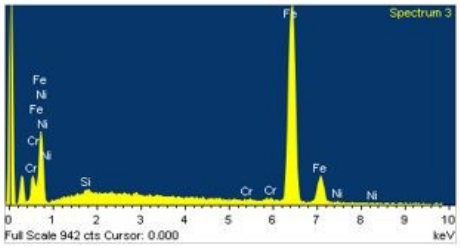

Figure 51: Chemistry, EDS spectrum, and area analysis of substrate of UWM Sample #5, cast at Maynard Steel. JOEL SEM, 27x, WD 12mm, accelerating voltage of 15 keV.

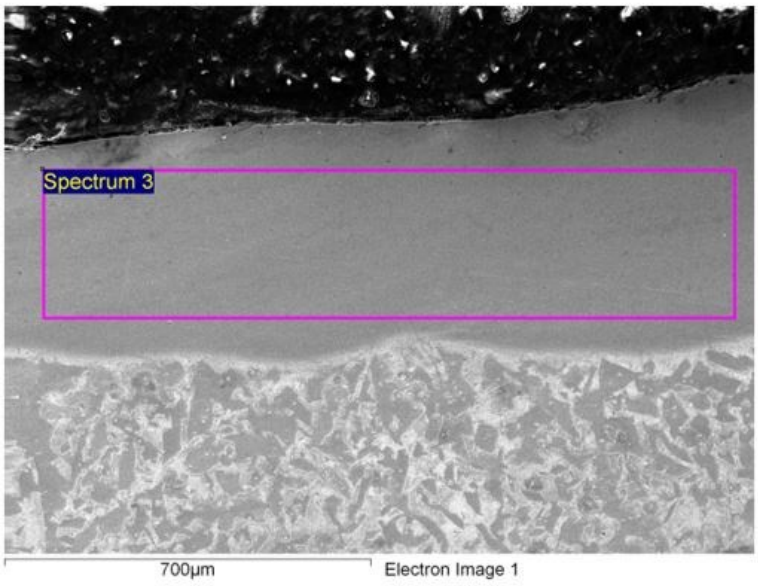

Sample #6

Element	Weight %	Atomic %
Fe	58.24	57.98
Ni	13.95	12.93
Cr	27.81	29.09
Total:	100	100

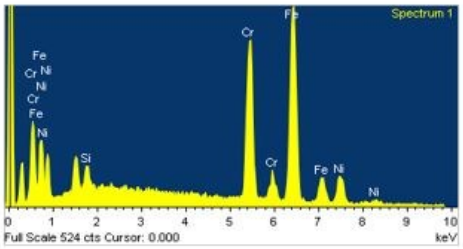

Figure 52: Chemistry, EDS spectrum, and area analysis of surface of UWM Sample #6, cast at Maynard Steel. JOEL SEM, 27x, WD 12mm, accelerating voltage of 15 keV.

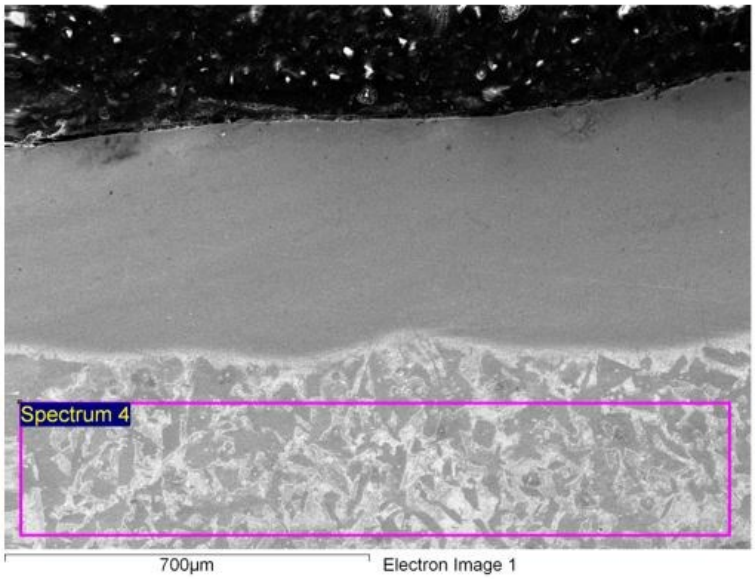

Sample #6

Element	Weight %	Atomic %
Fe	99.73	99.77
Ni	0.06	0.04
Cr	0.21	0.19
Total:	100	100

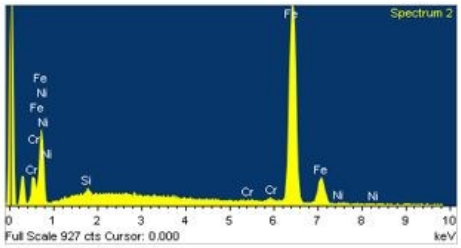

Figure 53: Chemistry, EDS spectrum, and area analysis of substrate of UWM Sample #6, cast at Maynard Steel. JOEL SEM, 27x, WD 12mm, accelerating voltage of 15 keV.

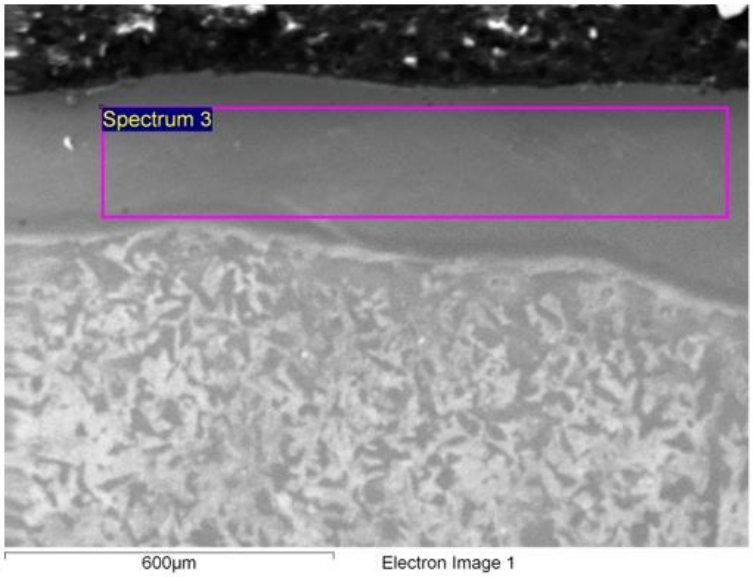

Sample #7

Element	Weight %	Atomic %
Fe	76.37	77.83
Ni	7.79	6.72
Cr	15.85	15.45
Total:	100	100

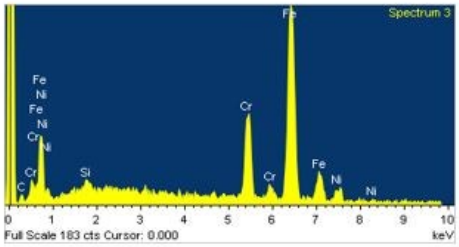

Figure 54: Chemistry, EDS spectrum, and area analysis of surface of Maynard Sample #7, cast at Maynard Steel. JOEL SEM, 27x, WD 12mm, accelerating voltage of 15 keV.

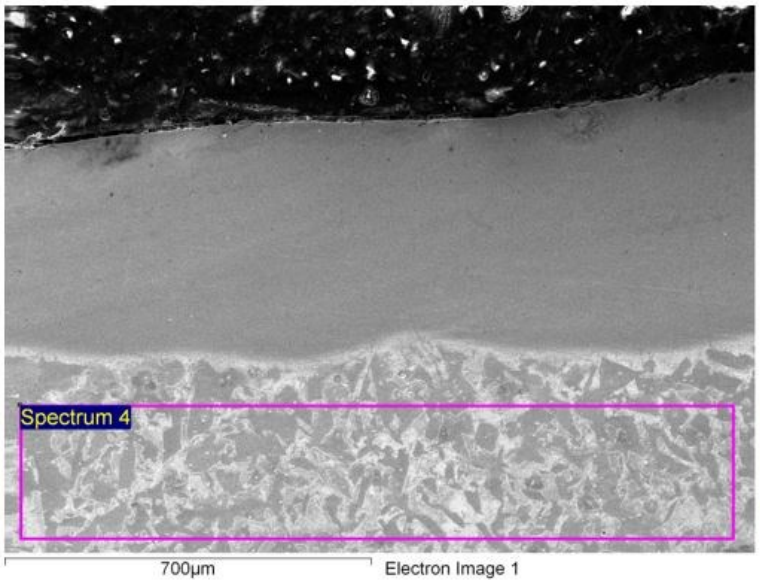

Sample #7

Element	Weight %	Atomic %
Fe	99.51	99.58
Ni	0.47	0.40
Cr	0.02	0.02
Total:	100	100

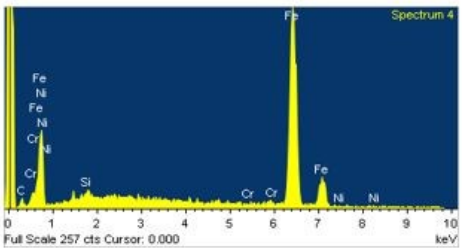

Figure 55: Chemistry, EDS spectrum, and area analysis of substrate of Maynard Sample #7, cast at Maynard Steel. JOEL SEM, 27x, WD 12mm, accelerating voltage of 15 keV.

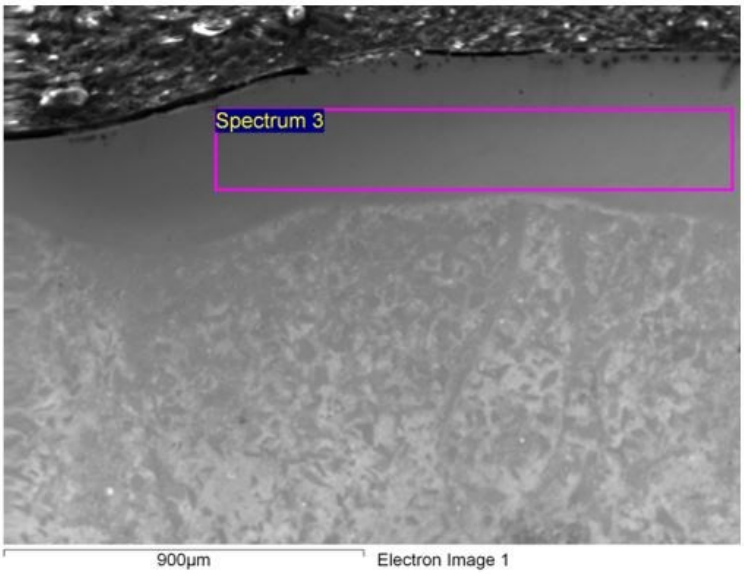

Sample #8

Element	Weight %	Atomic %
Fe	76.49	77.82
Ni	5.66	4.86
Cr	17.85	17.32
Total:	100	100

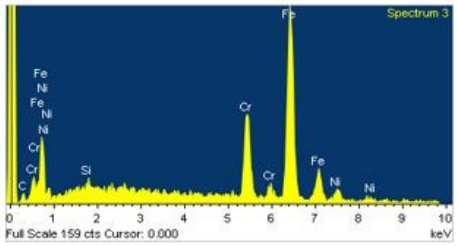

Figure 56: Chemistry, EDS spectrum, and area analysis of surface of Maynard Sample #8, cast at Maynard Steel. JOEL SEM, 27x, WD 12mm, accelerating voltage of 15 keV.

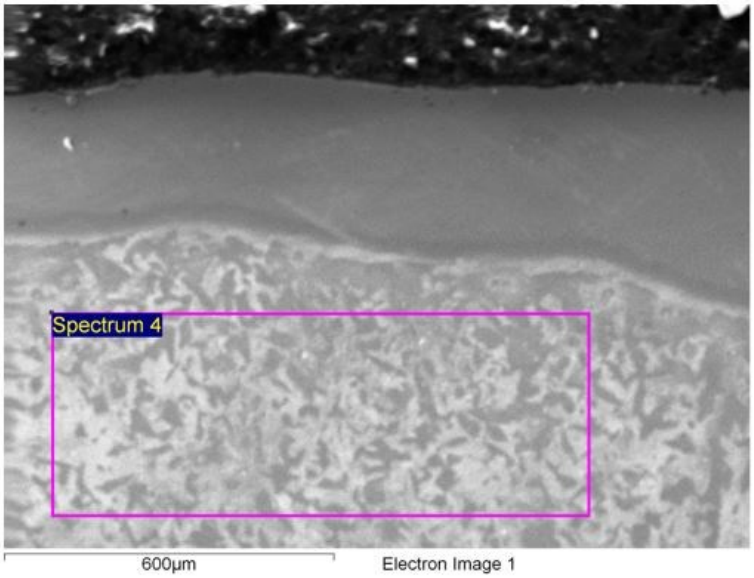

Sample #8

Element	Weight %	Atomic %
Fe	99.63	99.65
Ni	0.11	0.10
Cr	0.26	0.25
Total:	100	100

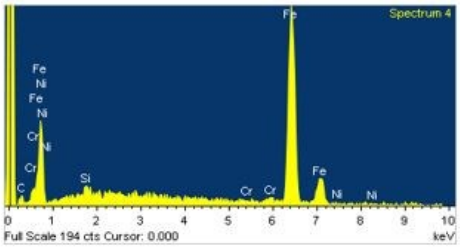

Figure 57: Chemistry, EDS spectrum, and area analysis of substrate of Maynard Sample #8, cast at Maynard Steel. JOEL SEM, 27x, WD 12mm, accelerating voltage of 15 keV.

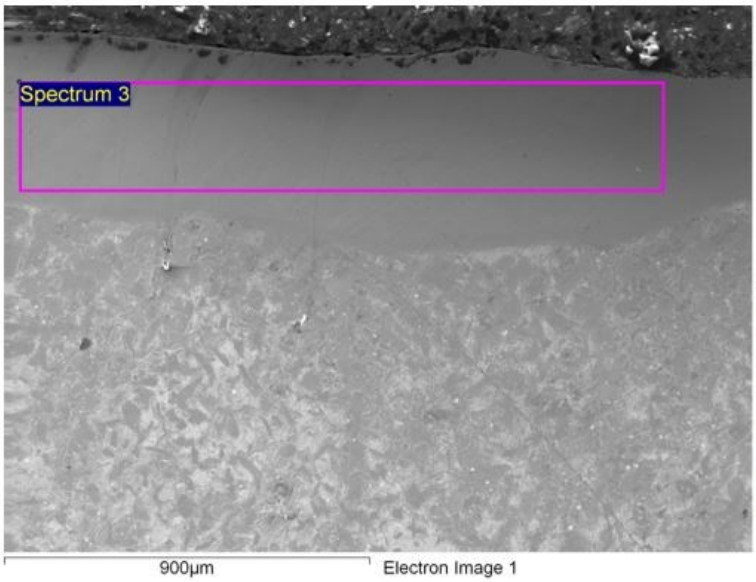

Sample #9

Element	Weight %	Atomic %
Fe	75.80	77.07
Ni	7.29	6.34
Cr	16.91	16.59
Total:	100	100

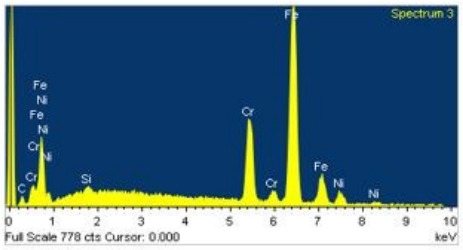

Figure 58: Chemistry, EDS spectrum, and area analysis of surface of Maynard Sample #9, cast at Maynard Steel. JOEL SEM, 27x, WD 12mm, accelerating voltage of 15 keV.

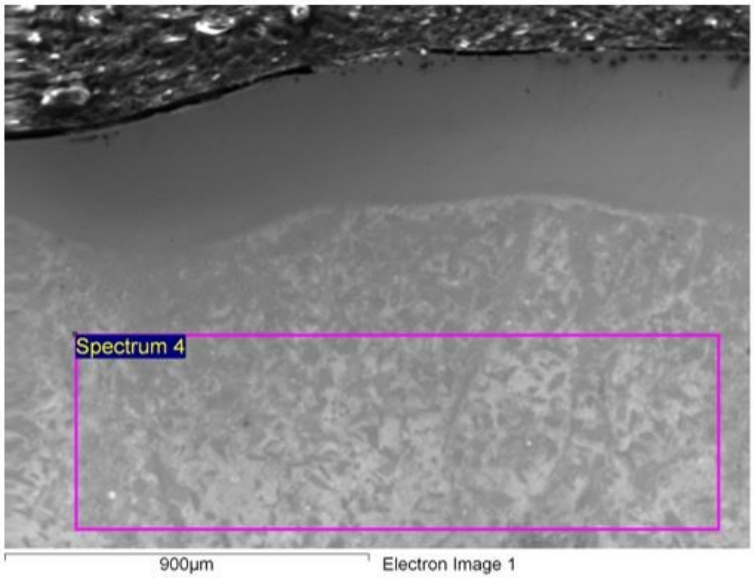

Sample #9

Element	Weight %	Atomic %
Fe	99.47	99.58
Ni	0.40	0.42
Cr	0.13	0.10
Total:	100	100

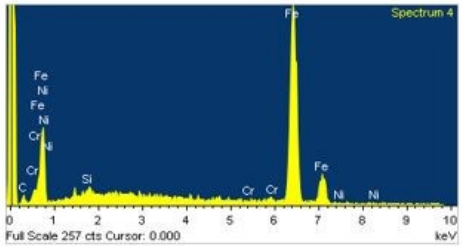

Figure 59: Chemistry, EDS spectrum, and area analysis of substrate of Maynard Sample #9, cast at Maynard Steel. JOEL SEM, 27x, WD 12mm, accelerating voltage of 15 keV.

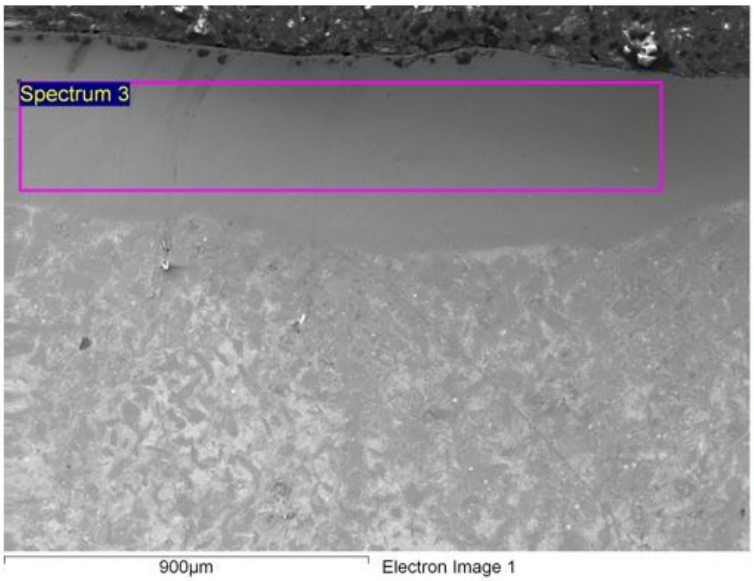

Sample#10

Element	Weight %	Atomic %
Fe	75.97	77.27
Ni	7.28	6.32
Cr	16.75	16.41
Total:	100	100

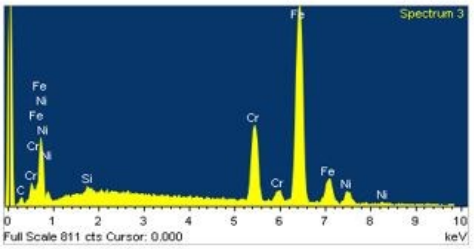

Figure 60: Chemistry, EDS spectrum, and area analysis of surface of Maynard Sample #10, cast at Maynard Steel. JOEL SEM, 27x, WD 12mm, accelerating voltage of 15 keV.

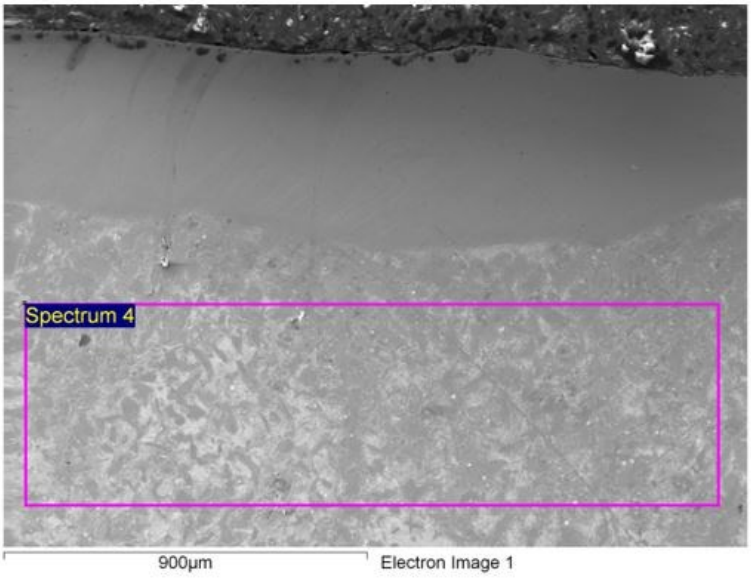

Sample#10

Element	Weight %	Atomic %
Fe	99.60	99.61
Ni	0.28	0.28
Cr	0.12	0.11
Total:	100	100

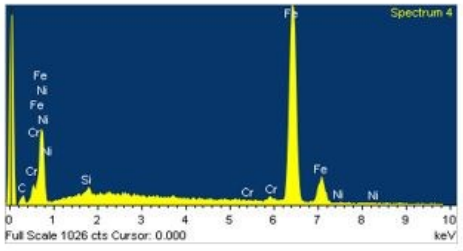

Figure 61: Chemistry, EDS spectrum, and area analysis of substrate of Maynard Sample #10, cast at Maynard Steel. JOEL SEM, 27x, WD 12mm, accelerating voltage of 15 keV

Appendix B

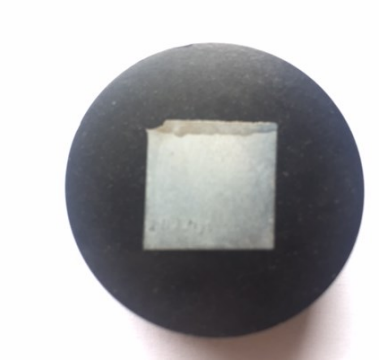

Figure 62: Maynard Sample #3. Ten Vickers Microhardness tests were taken in the enriched area, and ten were taken in the steel substrate.

Maynard Sample 3 Surface

Position	HV_{500}
1	390
2	427
3	416
4	408
5	397
6	401
7	412
8	404
9	399
10	412
Average	406.6

Maynard Sample 3 Substrate

Position	HV_{500}
1	149
2	154
3	155
4	143
5	159
6	164
7	160
8	148
9	162
10	145
Average	153.9

Figure 63: The Vickers Microhardnesses of the surface and substrate of Maynard Sample #3

Maynard Sample 4 Surface

Position	HV_{500}
1	399
2	388
3	410
4	403
5	418
6	420
7	396
8	404
9	417
10	384
Average	403.9

Maynard Sample 4 Substrate

Position	HV_{500}
1	147
2	149
3	158
4	142
5	159
6	160
7	153
8	157
9	140
10	158
Average	152.3

Figure 64: The Vickers Microhardnesses of the surface and substrate of Maynard Sample #4

Maynard Sample 5 Surface

Position	HV_{500}
1	388
2	392
3	413
4	401
5	387
6	394
7	406
8	392
9	408
10	398
Average	397.9

Maynard Sample 5 Substrate

Position	HV_{500}
1	159
2	154
3	149
4	147
5	152
6	155
7	161
8	151
9	147
10	149
Average	152.4

Figure 65: The Vickers Microhardnesses of the surface and substrate of Maynard Sample #5

Maynard Sample 6 Surface

Position	HV_{500}
1	384
2	424
3	389
4	405
5	410
6	401
7	413
8	397
9	399
10	387
Average	400.9

Maynard Sample 6 Substrate

Position	HV_{500}
1	147
2	154
3	155
4	143
5	160
6	157
7	155
8	143
9	148
10	146
Average	150.8

Figure 66: The Vickers Microhardnesses of the surface and substrate of Maynard Sample #6

Maynard Sample 7 Surface

Position	HV_{500}
1	482
2	487
3	490
4	486
5	492
6	479
7	483
8	482
9	492
10	489
Average	486.2

Maynard Sample 7 Substrate

Position	HV_{500}
1	148
2	159
3	158
4	152
5	149
6	153
7	158
8	149
9	155
10	153
Average	153.4

Figure 67: The Vickers Microhardnesses of the surface and substrate of Maynard Sample #7

Maynard Sample 8 Surface

Position	HV_{500}
1	479
2	491
3	477
4	483
5	482
6	492
7	482
8	493
9	490
10	483
Average	485.2

Maynard Sample 8 Substrate

Position	HV_{500}
1	158
2	153
3	158
4	149
5	155
6	147
7	159
8	158
9	161
10	158
Average	155.6

Figure 68: The Vickers Microhardnesses of the surface and substrate of Maynard Sample #8

Maynard Sample 9 Surface

Position	HV_{500}
1	490
2	492
3	479
4	478
5	486
6	482
7	477
8	493
9	481
10	487
Average	484.5

Maynard Sample 9 Substrate

Position	HV_{500}
1	146
2	152
3	154
4	155
5	148
6	159
7	157
8	155
9	149
10	153
Average	152.8

Figure 69: The Vickers Microhardnesses of the surface and substrate of Maynard Sample #8

Maynard Sample 10 Surface

Position	HV_{500}
1	484
2	487
3	492
4	486
5	479
6	478
7	481
8	484
9	487
10	478
Average	483.6

Maynard Sample 10 Substrate

Position	HV_{500}
1	156
2	155
3	149
4	157
5	149
6	152
7	150
8	155
9	158
10	155
Average	153.6

Figure 70: The Vickers Microhardnesses of the surface and substrate of Maynard Sample #7

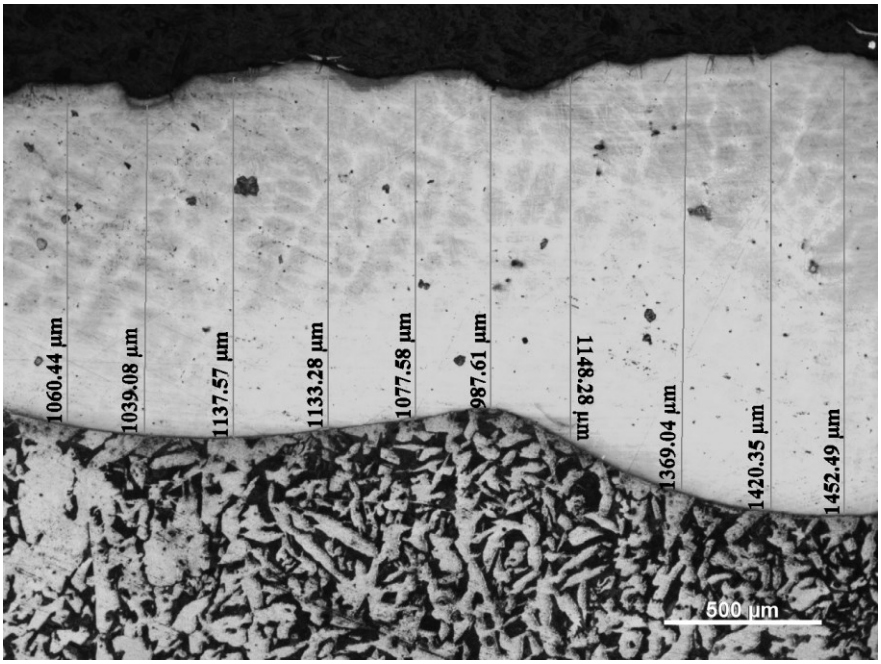

Figure 71: Optical image of enriched surface of Maynard Sample #3 at 50x magnification

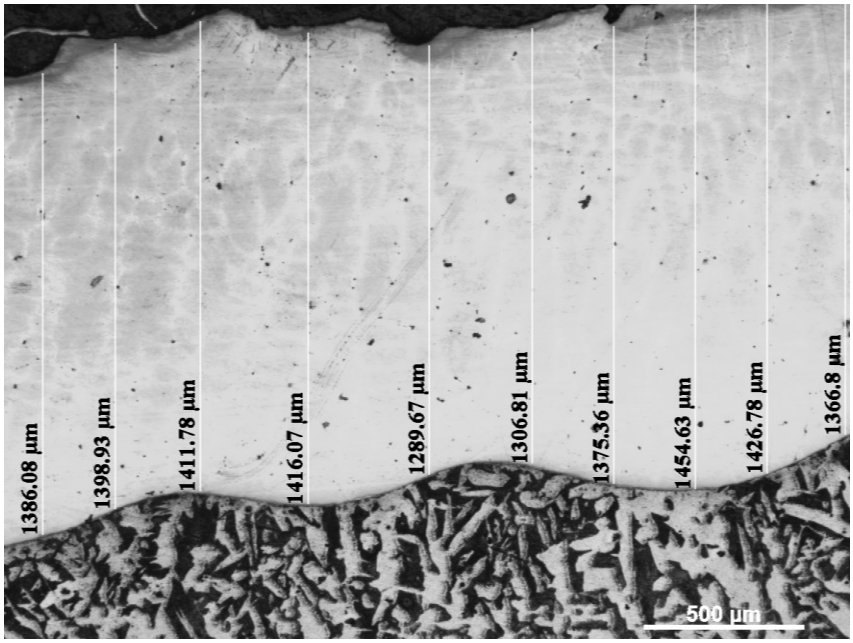

Figure 72: Optical image of enriched surface of Maynard Sample #4 at 50x magnification

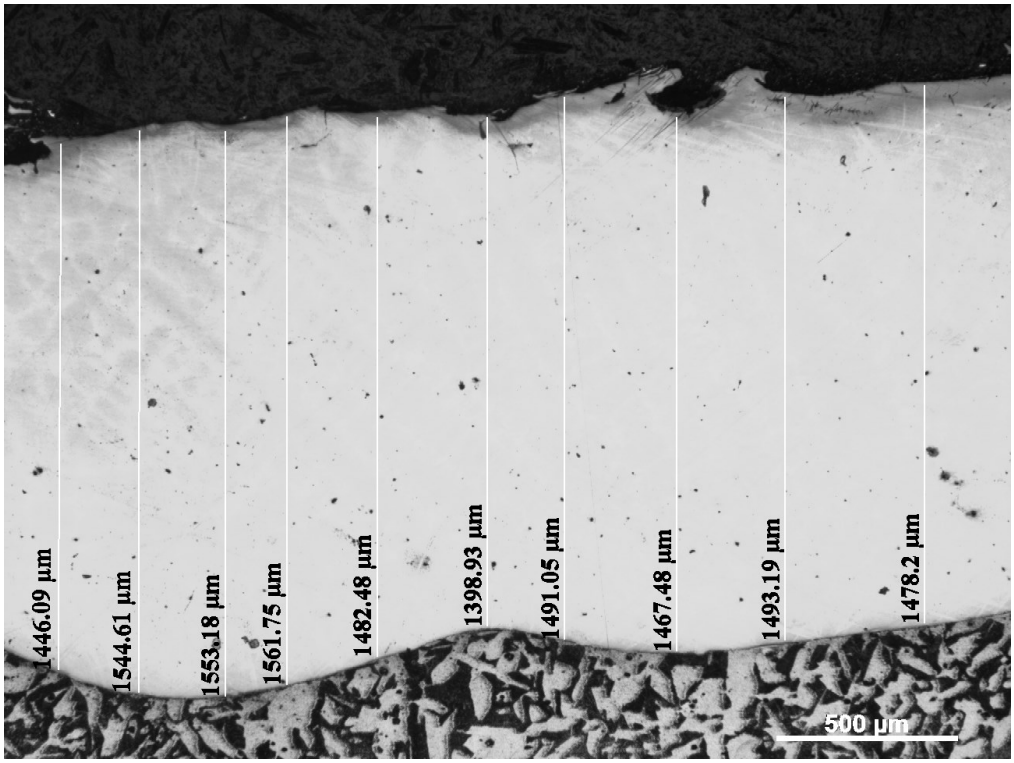

Figure 73: Optical image of enriched surface of Maynard Sample #5 at 50x magnification

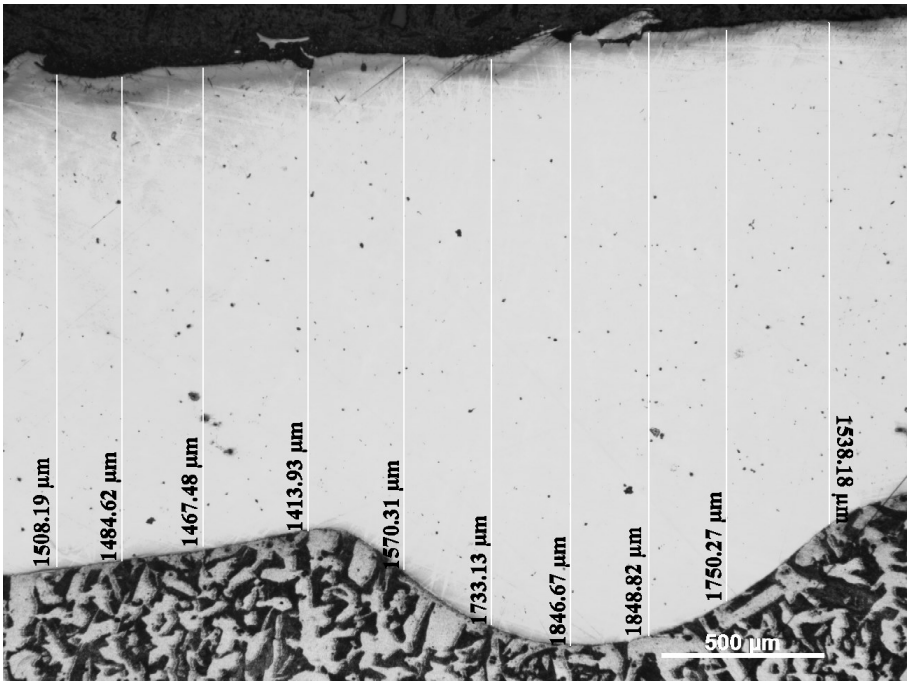

Figure 74: Surface measurements of Maynard Sample #6 at 100x magnification

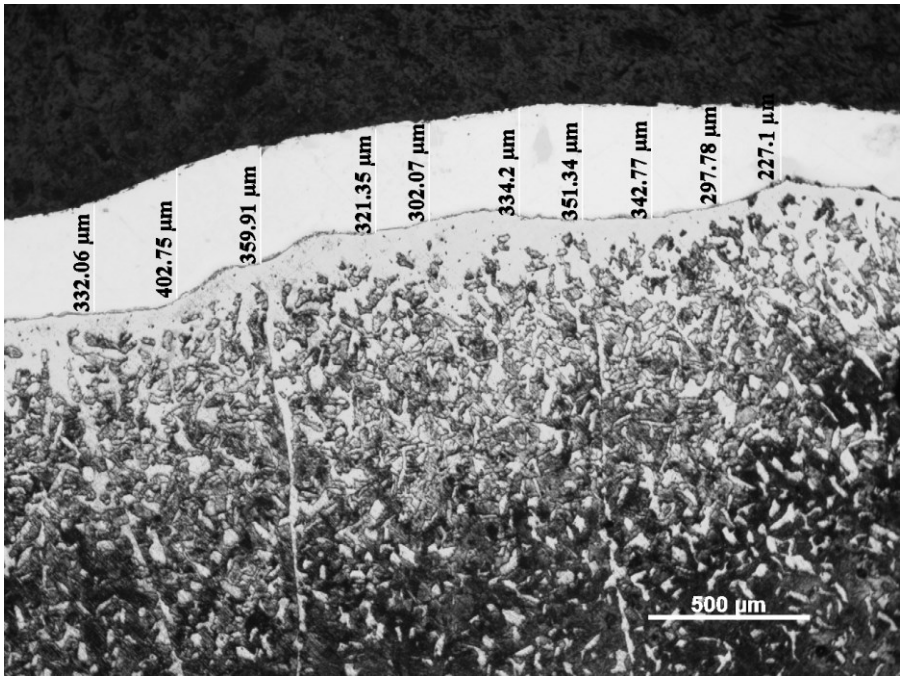

Figure 75: Surface measurements of Maynard Sample #7 at 100x magnification

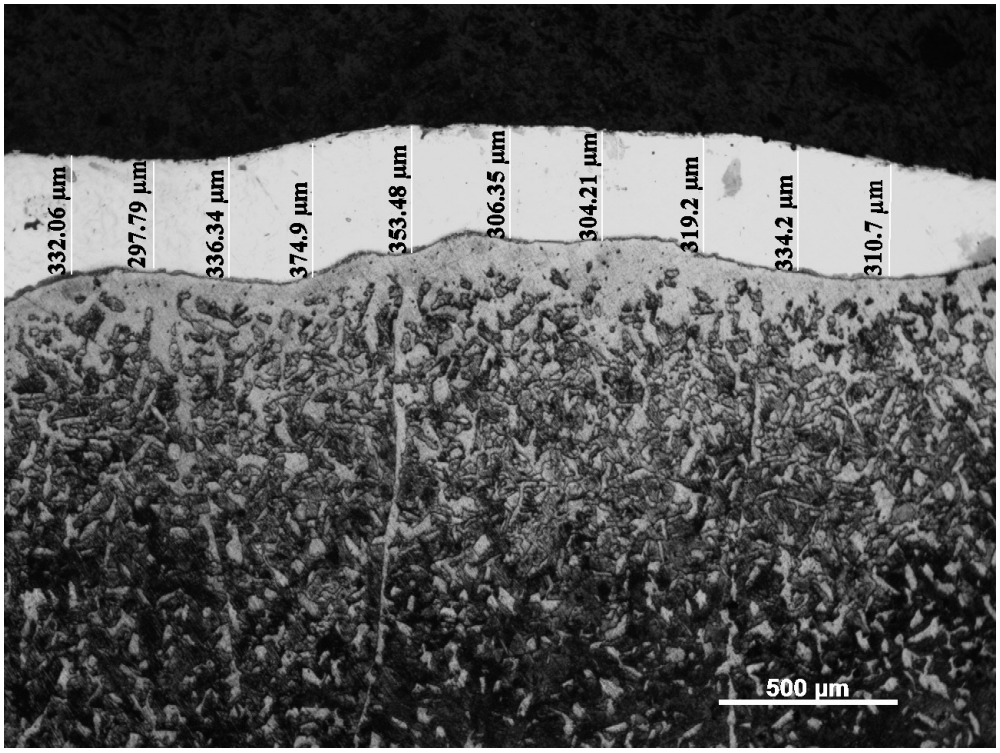

Figure 76: Surface measurements of Maynard Sample #8 at 100x magnification

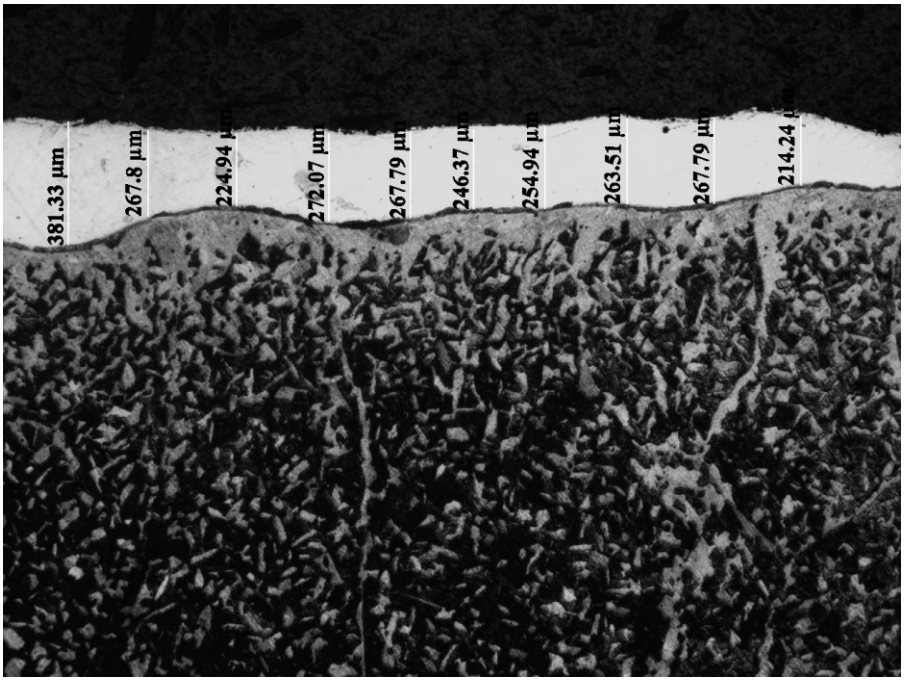

Figure 77: Surface measurements of Maynard Sample #9 at 100x magnification

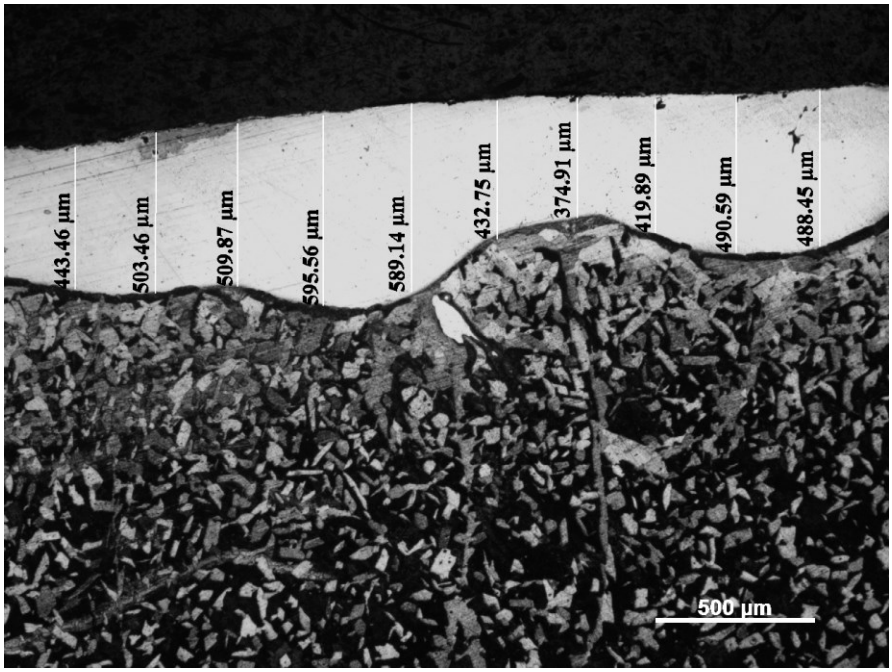

Figure 78: Surface measurements of Maynard Sample #10 at 100x magnification

Maynard Sample	Powders Added	Surface Comp. %	Surface Thickness	Hardness	Corrosion Rate
#1 (heat 1)	6g Ni, 0g Cu	WCB Steel	unmeasurable	unmeasurable	not measured
#2 (heat 1)	6g Ni, 3g Cu	WCB Steel	unmeasurable	unmeasurable	not measured
#3 (heat 2)	10g Ni	16.3 Ni, 83.2 Fe	1342 µm	406 HV_{500}	not measured
#4 (heat 2)	10g Ni	20.9 Ni, 78.6 Fe	1298 µm	403 HV_{500}	not measured
#5 (heat 2)	10g Ni	16.9 Ni, 82.9 Fe	1387 µm	397 HV_{500}	not measured
#6 (heat 2)	10g Ni	16.1 Ni, 83.4 Fe	1423 µm	400 HV_{500}	not measured
#7 (heat 3)	20g Cr, 8g Ni	15.8 Cr, 7.8 Ni, 76.7 Fe	342 µm	486 HV_{500}	0.066 mm/yr
#8 (heat 3)	20g Cr, 8g Ni	17.8 Cr, 5.7 Ni, 76.5 Fe	297 µm	485 HV_{500}	0.071 mm/yr
#9 (heat 3)	20g Cr, 8g Ni	16.9 Cr, 7.3 Ni, 75.8 Fe	319 µm	484 HV_{500}	0.087 mm/yr
#10 (heat 3)	20g Cr, 8g Ni	16.8 Cr, 7.3 Ni, 76 Fe	352 µm	483 HV_{500}	not measured

Figure 79: Chart summarizing results for the samples cast at Maynard Steel

UWM Sample	Powders Added	Surface Comp. %	Surface Thickness	Hardness	Corrosion Rate
#1	6g Ni, 0g Cu	WCB Steel	unmeasurable	not measured	not measured
#2	6g Ni, 3g Cu	WCB Steel	unmeasurable	not measured	not measured
#3	25g Cr, 10g Ni	39.3 Cr, 15.6 Ni, 45.1 Fe	unmeasurable	not measured	not measured
#4	25g Cr, 10g Ni	38.7 Cr, 14.2 Ni, 47.1 Fe	unmeasurable	not measured	not measured
#5	25g Cr, 10g Ni	39.7 Cr, 13.3 Ni, 47 Fe	unmeasurable	not measured	not measured
#6	25g Cr, 10g Ni	27.8 Cr, 13.9 Ni, 58.2 Fe	unmeasurable	not measured	not measured

Figure 80: Chart summarizing results for the samples made at UWM Laboratory